

2018

A MULTIPHYSICS COMPUTATIONAL FRAMEWORK FOR UNDERSTANDING CELL AND MICROTISSUE MORPHOGENESIS

Bahador Marzban
University of Rhode Island, ba.marzban@gmail.com

Follow this and additional works at: https://digitalcommons.uri.edu/oa_diss

Terms of Use

All rights reserved under copyright.

Recommended Citation

Marzban, Bahador, "A MULTIPHYSICS COMPUTATIONAL FRAMEWORK FOR UNDERSTANDING CELL AND MICROTISSUE MORPHOGENESIS" (2018). *Open Access Dissertations*. Paper 799.
https://digitalcommons.uri.edu/oa_diss/799

This Dissertation is brought to you by the University of Rhode Island. It has been accepted for inclusion in Open Access Dissertations by an authorized administrator of DigitalCommons@URI. For more information, please contact digitalcommons-group@uri.edu. For permission to reuse copyrighted content, contact the author directly.

A MULTIPHYSICS COMPUTATIONAL FRAMEWORK FOR
UNDERSTANDING CELL AND MICROTISSUE MORPHOGENESIS

BY

BAHADOR MARZBAN

A DISSERTATION SUBMITTED IN PARTIAL FULFILLMENT OF THE

REQUIREMENTS FOR THE DEGREE OF

DOCTOR OF PHILOSOPHY

IN

MECHANICAL ENGINEERING AND APPLIED MECHANICS

UNIVERSITY OF RHODE ISLAND

2018

DOCTOR OF PHILOSOPHY DISSERTATION
OF
BAHADOR MARZBAN

APPROVED:

Dissertation Committee:

Major Professor Hongyan Yuan

Arun Shukla

David Taggart

Li Wu

Nasser H. Zawia
DEAN OF THE GRADUATE SCHOOL

UNIVERSITY OF RHODE ISLAND
2018

ABSTRACT

A sophisticated computational model is developed to consider different interactive parts between cells and its components and their local microenvironment. The present work is mainly focused on the modeling of the coupling of the stress and concentration of the signaling proteins within the cell domain. In this research, the fundamental aspects and details of a coupled Contraction-Reaction-Diffusion (CRD), is presented. The model accounts for diffusion of the proteins and mechanical equilibrium of the cells simultaneously while considering different subunits which are affecting the cell migration. For instance, cell-cell interaction, nucleus effects, focal adhesion distribution, anisotropic stress fiber formation, membrane tension, microtubule structure, and growth and retraction of the cells are considered. Collectively, because of the interaction of these different subunits, the cell works as a single migratory machine. The model fills the gap in coupled biomechanical and biochemical models for the biological cells and predicts both the instantaneous and the long-term dynamic behavior of the cells. In order to evaluate the proposed computational cell model, biological experiments such as cell migration, durotaxis, and collective cell migration has been simulated using the proposed computational model. The proposed model presents a simple mechanistic understanding of mechanosensing of substrate stiffness gradient at the cellular scale, which can be incorporated in more sophisticated mechanobiochemical models to address complex problems in mechanobiology and bioengineering. The proposed model and computer program is able to simulate long-term interaction of hundreds of cells with each other

(e.g. cell-cell contact) and with the elastic substrate on a desktop workstation efficiently.

ACKNOWLEDGMENTS

I would first like to acknowledge my advisor, Prof. Hongyan Yuan, for all of his guidance and support through this project. His mentoring has helped me to grow as a scientist and individual through the last few years. He taught me to expand my knowledge in scientific research and in life and for that I am very grateful. Furthermore, I would like to thank my committee members Prof. Arun Shukla, Prof. Li Wu and Prof. David Taggart for their continued guidance and support during this process. Their patience and insight has been motivating and heartwarming and I am grateful for this. I would like to thank Prof. Datsaris, I was serving as his teaching assistant during last 2 years and I learned a lot from him. Along with my committee, I would like to thank my lab mates and friends Carlos Javier, Ralph Kfourri, Shyamal Kishore, and Richard Sperling for their continued presence throughout the course of my research. I would also like to thank Jen Cerullo, Nancy Santucci and the rest of the mechanical engineering department faculty and staff.

I must also thank my family, my father and mother, Abolghasem and Golchehreh Marzban, who encouraged me toward my goals by their hearts, my dear brother, Babak Marzban and my beloved sisters, Laleh, Bahare, Fatemeh and Zahra for their non-stop love and support. Special thank to my dear uncles Prof. Hassan Marzban and Dr. Asghar Marzban for their supports. I would like to thank my friends at URI, Hadi Hosseini, Sanaz Motamedi, Mino Madani, Faramarz Joodaki, Nasim Ganji, Mohammad Moein Safaee, Negar Rahmani, Shahab Ilbeigi, Nasim Rahmani, and Vida Karimnia for their presence through all of the moments from small victories to all the challenges. Special thanks to my friends Hassan Hosseini and Mojtaba Oshrieh.

Dedication

This humble work is dedicated to my parents, Abolghasem and Golchehreh Marzban, who have always loved me unconditionally and whose good examples have taught me to work hard for the things that I aspire to achieve. I am truly thankful for having you in my life.

PREFACE

The following studies focus on the gap in the mathematical modeling for cell mechanics and cell motility. The manuscript formatting has been adopted for this dissertation.

Chapter 1 is an introduction to the subject of cell migration and also this chapter provides a brief review of the previous research on mathematical modeling of cell migration.

Chapter 2 seeks to propose a minimal mathematical model for explaining the durotaxis, a rigidity driven cell migration. It is shown that how the difference in traction can justify the durotaxis. This chapter will follow the formatting guidelines specified by Biomechanics and modeling in mechanobiology.

Chapter 3, focused on developing the model from a static model to a whole-cell dynamic model by considering the signaling feedback (i.e. protrusion and retraction). Using the model, durotaxis a rigidity driven cell migration has been simulated. This chapter will follow the formatting guidelines specified by Biophysical Journal.

The next study in Chapter 4, focused on developing the model from a single cell model to a multicellular dynamic model by considering the cell-cell adhesion module and cell-cell interaction. Using the developed model, experimental scenarios such as tissue ring cell monolayer has been simulated. This chapter will follow the formatting guidelines specified by PLOS ONE computational biology.

In Chapter 5 we will discuss the conclusion and the future work of the research.

TABLE OF CONTENTS

ABSTRACT	ii
ACKNOWLEDGMENTS	iv
Dedication	v
PREFACE.....	vi
TABLE OF CONTENTS.....	vii
LIST OF TABLES	xi
LIST OF FIGURES	xii
CHAPTER 1	1
INTRODUCTION AND LITERATURE REVIEW.....	1
References	4
CHAPTER 2:	7
A MINIMAL MECHANICS MODEL FOR MECHANOSENSING OF SUBSTRATE RIGIDITY GRADIENT IN DUROTAXIS.....	7
ABSTRACT	8
Introduction.....	8
Model description.....	14
1D Model	14
2D Model	17
Results	17
1D cell, when $\alpha = 1$	17
1D cell, when $\alpha > 1$	18
Computational results for 2D cells	21
Conclusions	24

Acknowledgments	24
Compliance with ethical standards	25
Conflicts of interest	25
References	25
CHAPTER 3:	33
A contraction-reaction-diffusion model for cell migration: integrating	
biomechanics and biochemistry at the whole cell level.....	33
ABSTRACT	34
Introduction	34
Model Description	37
Cytoskeleton module.....	38
The elasticity model of the cytoskeleton	38
Stress-fiber structure tensor	40
Cell motility module.....	41
Reaction-diffusion of protrusion and retraction signals	41
Movement of the cell (i.e., protrusion and retraction).....	43
Cytoskeletal asymmetry.....	43
Cell-substrate interaction module	44
Numerical implementation of the model.....	45
Mechanosensing at the whole-cell scale.....	46
Simulation results.....	47
Establishment of polarity of the cell with the reaction-diffusion submodel	47
Focal adhesion stress-dependent protrusion signal distribution	51
The role of the cytoskeleton asymmetry to the persistent migration	52
Comparison with experimental data.....	54
Simulation of durotaxis	57

Cell shape.....	60
Conclusions.....	62
Acknowledgments	63
References	63
CHAPTER 4 :	67
RDC-CELL: A computational model and package for whole-cell multiphysics	
simulations of cell monolayer	67
Abstract.....	68
Introduction	68
Model Description	70
Physical and mathematical domains.....	70
Nucleus deformation and movement.....	72
Cell-cell interaction module	73
Mechanobiochemical coupling	73
Numerical Implementation	74
Case study: Collective cell migration in monolayer tissue	78
Conclusions	79
Acknowledgments	80
References	80
CHAPTER 5 :	88
Conclusions and Future Work.....	88
Conclusions	88
Future Work.....	88
Extending the Model to 3Dimensional Model	89
Parameter space search.....	89
Appendix A (Major subroutines).....	92

Appendix B (Variables)	97
BIBLIOGRAPHY	100

LIST OF TABLES

Chapter 3:

Table 1. Characteristic cell shape simulated by the cell model..... 61

Appendix B:

Table 1. Parameter used in the simulations. Some of the variables derived from the literature and the rest are the estimated parameter. 98

LIST OF FIGURES

Chapter 2:

Figure 1 Previous experimental observations on single-cell mechanosensing. (a) The phenomenon of durotaxis (reprinted with permission from [1]): a cell crawls from the stiffer side of the substrate toward the softer side and turned 90° at the interface (the dotted line is an approximation of the rigid-to-soft interface). (b) Traction stress under a circular cell crossing step-rigidity boundary (reprinted with permission from [14]) (c) Lamellipodia extension in a square cell (reprinted with permission from [15]). 9

Figure 2. (a) Schematic representation of a single-cell model by Marcq et al. [29], where the cell adheres to the substrate only at the two ends. (b) Schematic representation of our single-cell model where the cell adheres to the substrate in the whole cell domain. The left half of the cell adhere to a soft region, while the right half of the cell adheres to a stiff region of the substrate. The cytoskeleton is composed of a passive spring and an active contractile element. Note that the FA and substrate springs, although drawn in a vertical direction, resist displacement in the horizontal direction in the 1D and 2D model. 14

Figure 3. (a) Traction stress (scaled by σ_c) reaches a plateau at large substrate rigidity (in units of kPa/ μm). (b) Analytical solution of traction stress T_x . (c) Analytical solution of cytoskeletal stress σ_x . Parameter values used: $L = 20 \mu\text{m}$, $k_{FA}=1 \text{ kPa}/\mu\text{m}$, $k_s=0.1 \text{ kPa}/\mu\text{m}$, $h=3 \mu\text{m}$, $\sigma_c=4 \text{ kPa}$, $\alpha = 3$, and $E=4 \text{ kPa}$. These parameter values are used for the remainder of the paper unless specifically mentioned. 19

Figure 4. (a) Traction stress difference ΔT_x as a function of α for different values of E when $k_s=0.1$ kPa/ μm . (b) $\Delta T_x/T_{\text{max}}$ as a function of α for different values of k_s when $E=2$ kPa..... 21

Figure 5. Finite element model predictions for 2D cells. (a) Displacement and traction stress of a circular cell crossing a step-rigidity boundary. (b) Traction stress for the square cell. (c) Traction stress distributions of the cell shown in Fig. 1a at the sequential time instants. (Parameter values used: $G=2.3$ kPa, $K=5$ kPa, cell area is $500 \mu\text{m}^2$, other parameters are the same as 1D analytical model given in Fig. 3)..... 23

Chapter 3:

Figure 1. Schematic illustrations of cell migration on a 2D surface. A) Side view, B) Top view. C) Physical domains defined in the cell model..... 37

Figure 2. Block diagram for the model, note that numbers in parentheses are equation numbers..... 47

Figure 3. Establishment of polarity of the cell with the reaction-diffusion submodel. (A) In a circular cell, protrusion signal ξ polarizes spontaneously with random initial perturbation. (B) The effect of cell shape on the spatial patterns of protrusion signal in an elliptical cell. (C)-(F) Effect of modal parameters ζ_a , ζ_0 , K_0^ξ , and K_{off}^ξ on the steady-state distribution of protrusion signal ξ . Note that all the panels share the same color bar. 50

Figure 4. The effect of mechanobiochemical coupling to the protrusion signal. (A) Protrusion signal ξ forms gradient pattern spontaneously with random initial perturbation. (B) Traction stress contour, with coupling protrusion signal. (C)

Protrusion signal ξ forms circular pattern, with coupling traction stress, (i.e., turning on stress dependent activation parameter, $K_T^\xi = 0.45$)..... 52

Figure 5. The role of the cytoskeleton asymmetry to the persistent migration. The first and third rows: protrusion signal. The second and fourth rows: traction stress. For the first 2 row the Microtubule effect is simply turned off by setting the $K_M^\rho = 0$ and $K_M^\xi = 0$ For the third and fourth row, we just simply turned on the microtubule by setting $K_M^\rho = 0.1$ and $K_M^\xi = 0.05$ 54

Figure 6. Experimental results using micropillar test. The scale bars in the experimental figures are 10 um. The upper limit for the color bar for both experimental and simulation figures are 1 nN. 56

Figure 7. Simulation of durotaxis. The first and third rows: protrusion signal. The second and fourth rows: traction stress. Top two rows: higher stress dependent parameter, $K_T^\xi=0.6$, durotaxis happens. Bottom two rows: lower stress dependent, $K_T^\xi=0.4$, cell passes the interfaces. 59

Chapter 4:

Figure 1. Schematic illustrations of the cell model. (A) Schematic of cytoskeleton of the cell and main components of the cell’s structure. (B) Schematic illustrations of the physical domains in the cell model and cell–cell interaction. (C) The mechanobiochemical coupling and feedback loops in the cell morphogenesis model.72

Figure 2. Detailed flow chart of the cell monolayer algorithm..... 77

Figure 3. Collective cell migration in confluent monolayers. (A) Simulation snapshots of cells in confluent monolayers without cell-cell adhesion, (B) Simulation snapshots

of cells in confluent monolayers with cell-cell adhesion. Four subfigures in each row show protrusion signal, focal adhesion, traction stress, and stress fiber, respectively. In the stress fiber figures, fourth column, circles on the cells are the nucleus. Parameter value used: $k_{cc} = 1 \text{ kPa}$ 79

Chapter 5:

Figure 1. Flowchart of the genetic algorithm for parameter space search. 91

CHAPTER 1

INTRODUCTION AND LITERATURE REVIEW

Cell morphogenesis is a fundamental process in tissue formation. One of the challenges in the fabrication of living tissues in vitro is to recapitulate the complex morphologies of individual cells. Nowadays, because of the lack of knowledge for building tissues with embedded life-sustaining vascular networks, 3D printing of the human tissues more than a millimeter in size is subject to the failure. In 3D bioprinting, cells crawl and migrate in engineered microenvironments to form tissues. With computational simulations of cell migration and microtissue formation, optimal extracellular matrices can be designed to facilitate the recapitulation of micro-morphologies of tissues at the cellular resolution in 3D bioprinting. Simulations are efficient tools for evaluating and optimizing the feasibility of specific designs.

It has been shown that mechanical and external forces play a key role in biological cells and their motility. Lo et al. reported the substrate rigidity-based cell migration, they discovered that fibroblast cells make a 90 degree turn at the boundary of the soft and rigid zones of the extra cellular matrix (ECM); this is referred to as durotaxis [1]. Barnhart et al. showed that the level of adhesion to substrate affects morphologies of the cells [2]. Kim et al. observed that a group of endothelial cells tend to fill the empty spaces of the substrate by exerting force and pulling out traction in the direction of empty spaces, which is called Kenotaxis [3]. All of the above-mentioned phenomena are a few of many instances of the biomechanical behavior of

the biological cells. In general, mechanosensing is an interaction which is involved in a variety of biological processes such as cancer metastasis, wound healing, tissue formation, and embryological development.

Advancement of microscopy and cell imaging techniques including 2D and 3D force microscopy [4], multiple speckle microscopy [5] and monolayer stress microscopy [6] has enabled researchers to evaluate the mathematical models in cell mechanics considering the quantitative experimental data as the benchmark. In this context, developing a whole-cell mathematical model presents an ongoing challenge and has been the topic of intensive researches. For capturing the polarization of the cells during the cell migration (i.e., formation of the head and tail); inspired by Turing's instability; some studies used the reaction diffusion of biochemical molecules [7], [8], [9], [10]. Although these models were able to mimic the polarization, they did not consider the invisible mechanosensing of the biological cells. Zaman et al. considered the cells as a material point and were able to capture the motility behavior of a single cell in different stiffnesses of the ECM (i.e., higher stiffness associated with lower migration speed and lower stiffness associated with higher migration speed). However, their model cannot resolve the spatial distribution of the field variables such as traction stress, displacement and protrusion concentration within the single-cell domain [11]. Vernerey et al. proposed a static and rigidity sensitive cell model that can predict the stress fiber direction successfully [12]. A dynamic multi-cellular model is needed to consider the cell-cell interaction, effect of nucleus as well as the dynamic growth of the boundary at the front of the cell. Borau et al. presented a one-dimensional model which focuses on the rigidity sensing of the cells and yet it is

unable to consider the membrane tension, polarization, cell-cell interaction, and cell growth [13]. While each of the abovementioned models contributes to a better understanding of the cells behavior, lack of the studies on the biomechanics and biochemistry couplings of cell-microenvironment interactions has been identified, particularly computational models and methods that can describe and predict the dynamic process of microtissue formation.

Previously, our research was focused on developing a mechanical model for bio-hybrid cell contractility assays and studying the effect of thermal fluctuation on cell adhesion [14], [15]. In this study, an efficient and robust computational biomechanics model and software platform will be developed to simulate the dynamics of living cells at the whole-cell level. The proposed model establishes a firm link between protein distribution pattern and the traction stress in the cells. Specific biomechanics phenomenon including cell crawling and morphogenesis of cell monolayer tissues has been studied using the computational model.

The developed model integrates the biochemical and mechanical activities within individual cells spatiotemporally and it is mainly composed of four modules: mechanics of cytoskeleton, cell motility, cell-substrate interaction, and cell-cell interaction. In the cell membrane and cytosol domain reaction-diffusion equations of active and inactive diffusive molecules is formulated to model the protrusion and retraction protein concentrations. In the cytoskeleton domain elasticity equations is developed, and the mechanical stresses experienced by the cell has been solved. Finite element method (FEM) has been used to model the irregular shapes of cells and to

solve the resulting system of reaction-diffusion-elasticity equations. The weak coupling scheme between traction and protrusion and retraction protein concentrations has been adopted for this multiphysics problem. Automated mesh generation has been hired for re-meshing and to handle the element distortion in FEM due to the large shape changes of the cells.

References

- [1] C. M. Lo, H. B. Wang, M. Dembo, and Y.-L. Wang, “Cell movement is guided by the rigidity of the substrate,” *Biophys. J.*, vol. 79, pp. 144–152, 2000.
- [2] E. L. Barnhart, K. C. Lee, K. Keren, A. Mogilner, and J. A. Theriot, “An adhesion-dependent switch between mechanisms that determine motile cell shape,” *PLoS Biol.*, vol. 9, no. 5, 2011.
- [3] J. H. Kim *et al.*, “Propulsion and navigation within the advancing monolayer sheet,” *Nat. Mater.*, vol. 12, no. 9, pp. 856–863, 2013.
- [4] C. Franck, S. A. Maskarinec, D. A. Tirrell, and G. Ravichandran, “Three-Dimensional Traction Force Microscopy: A New Tool for Quantifying Cell-Matrix Interactions,” *PLoS One*, vol. 6, no. 3, p. e17833, 2011.
- [5] D. Dormann and C. J. Weijer, “Imaging of cell migration,” *EMBO J.*, vol. 25, no. 15, pp. 3480–3493, 2006.
- [6] D. T. Tambe *et al.*, “Monolayer Stress Microscopy: Limitations, Artifacts, and Accuracy of Recovered Intercellular Stresses,” *PLoS One*, vol. 8, no. 2, 2013.
- [7] M. Otsuji, S. Ishihara, C. Co, K. Kaibuchi, A. Mochizuki, and S. Kuroda, “A mass conserved reaction-diffusion system captures properties of cell polarity,”

- PLoS Comput. Biol.*, vol. 3, no. 6, pp. 1040–1054, 2007.
- [8] Y. Mori, A. Jilkine, and L. Edelstein-Keshet, “Wave-pinning and cell polarity from a bistable reaction-diffusion system.,” *Biophys. J.*, vol. 94, no. 9, pp. 3684–3697, 2008.
- [9] A. F. M. Marée, V. A. Grieneisen, and L. Edelstein-Keshet, “How cells integrate complex stimuli: The effect of feedback from phosphoinositides and cell shape on cell polarization and motility,” *PLoS Comput. Biol.*, vol. 8, no. 3, 2012.
- [10] A. F. M. Marée, A. Jilkine, A. Dawes, V. A. Grieneisen, and L. Edelstein-Keshet, *Polarization and movement of keratocytes: A multiscale modelling approach*, vol. 68, no. 5. 2006.
- [11] M. H. Zaman, R. D. Kamm, P. Matsudaira, and D. a Lauffenburger, “Computational model for cell migration in three-dimensional matrices,” *Biophys J*, vol. 89, no. 2, pp. 1389–1397, 2005.
- [12] F. J. Vernerey and M. Farsad, “A constrained mixture approach to mechanosensing and force generation in contractile cells,” *J. Mech. Behav. Biomed. Mater.*, vol. 4, no. 8, pp. 1683–1699, 2011.
- [13] C. Borau, R. D. Kamm, and J. M. García-Aznar, “A time-dependent phenomenological model for cell mechano-sensing,” *Biomech. Model. Mechanobiol.*, vol. 13, no. 2, pp. 451–462, 2014.
- [14] B. Marzban and H. Yuan, “The effect of viscous force on the prediction of muscle contractility in biohybrid cantilever-based experiments,” *Extrem. Mech. Lett.*, vol. 9, pp. 342–346, 2016.

- [15] B. Marzban and H. Yuan, “The effect of thermal fluctuation on the receptor-mediated adhesion of a cell membrane to an elastic substrate,” *Membranes (Basel)*, vol. 7, no. 2, 2017.

CHAPTER 2:
A MINIMAL MECHANICS MODEL FOR MECHANOSENSING OF
SUBSTRATE RIGIDITY GRADIENT IN DUROTAXIS

by

Bahador Marzban, Xin Yi, Hongyan Yuan

Has been published in Biomechanics and Modeling in Mechanobiology

*Corresponding Author:

Hongyan Yuan

Department of Mechanical, Industrial and Systems Engineering,

University of Rhode Island,

331A Pastore Hall, 51 Lower College Road, Kingston, RI

02881, USA

USA phone: +1-401-874- 2774

Email: hongyan_yuan@uri.edu

ABSTRACT

Durotaxis refers to the phenomenon in which cells can sense the spatial gradient of the substrate rigidity in the process of cell migration. A conceptual two-part theory consisting of the focal adhesion force generation and mechanotransduction has been proposed previously by Lo et al. to explain the mechanism underlying durotaxis. In the present work, we are concerned with the first part of the theory: how exactly is the larger focal-adhesion force generated in the part of the cell adhering to the stiffer region of the substrate? using a simple elasticity model and by assuming the cell adheres to the substrate continuously underneath the whole cell body, we show that the mechanics principle of static equilibrium alone is sufficient to account for the generation of the larger traction stress on the stiffer region of the substrate. We believe that our model presents a simple mechanistic understanding of mechanosensing of substrate stiffness gradient at the cellular scale, which can be incorporated in more sophisticated mechanobiochemical models to address complex problems in mechanobiology and bioengineering.

Introduction

It has been shown that biological cells can sense and respond to a variety of mechanical cues of their microenvironment, such as matrix rigidity [1], matrix topology [2], matrix dimensionality [3], shear flow [4], interstitial flow [5], cell-cell and cell-matrix adhesions [6], and cell shape constraints [7]. These mechanical stimuli play a critical regulatory role in many biological functions such as cell proliferation

[8], cell motility [1], [7], and differentiation [9]. Understanding the mechanisms underlying mechanosensing has become the focus of intensive experimental and theoretical studies [10]–[13]. In the present study, we are interested in durotaxis, a term coined by Lo et al. [1], which refers to the substrate rigidity-guided cell migration. They showed that (see Fig. 1a) when a fibroblast cell crawled from the stiffer side (i.e., the darker region) of the substrate toward the softer side (i.e., the brighter region), the cell made a 90-degree turn at the interface.

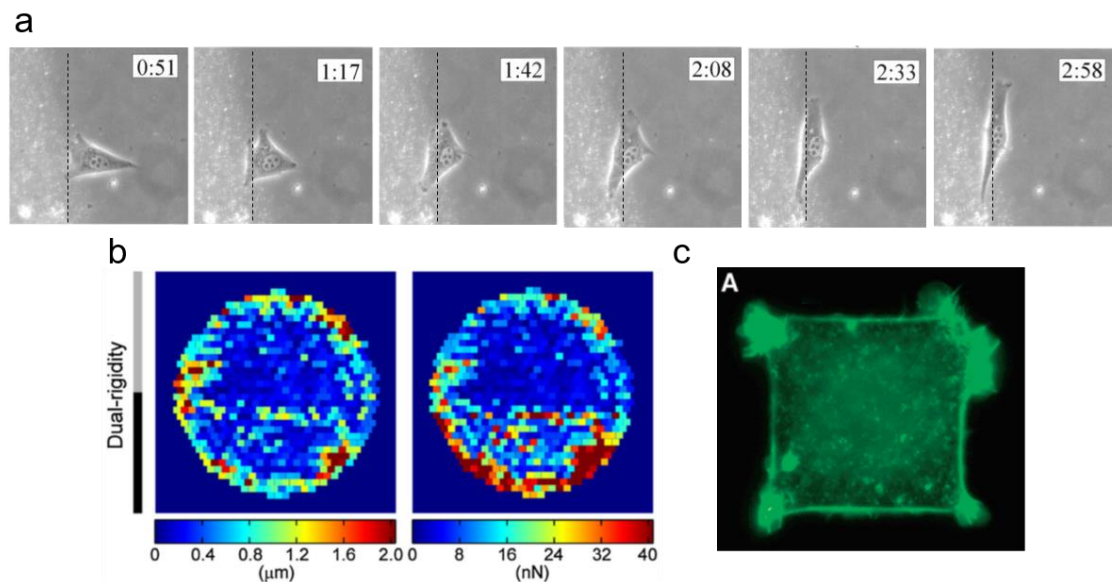


Figure 1 Previous experimental observations on single-cell mechanosensing. (a) The phenomenon of durotaxis (reprinted with permission from [1]): a cell crawls from the stiffer side of the substrate toward the softer side and turned 90° at the interface (the dotted line is an approximation of the rigid-to-soft interface). (b) Traction stress under a circular cell crossing step-rigidity boundary (reprinted with permission from [14]) (c) Lamellipodia extension in a square cell (reprinted with permission from [15]).

Because the importance of durotaxis in physiology and pathology, the molecular and subcellular mechanisms underlying mechanotransduction has attracted considerable attention [16]–[19]. Biomechanics models where single cells and cell-substrate linkages were modeled as elastic springs or elasticity theory, have been developed to account for rigidity sensing [13], [20], [21]. These models were only applied to the scenario where the individual cell was treated either as a point mass [20] or an small volume element [21]. In a series of studies [22]–[24], by modeling the individual cells or stress fibers as force dipoles distributed in continuum elastic 2D or 3D substrates, the researchers developed biomechanics models to interpretate mechanosensing mechanisms and to study the effect of mechanosensing on cell shape, stress fiber orientation, and synchronized beating of cardiomyocytes. On the other hand, the effect of durotaxis on cell migration dynamics on the long time have also been studied. For example, in the cell migration model by [25], substrate rigidity-dependence is taken into account by assuming focal adhesions are correlated with substrate stiffness. In the single cell migration model by [26], substrate rigidity-dependence is considered by assuming differential cell-substrate adhesions strength on substrates with different rigidity. Thus, in these durotaxis models, substrate-rigidity-dependence is used as the assumption in the cell migration models. To the best of our knowledge, in previous models, the spatial distribution of the substrate rigidity within the single cell domain is constant. The substrate rigidity is either changed for the whole cell or changed only when the cell moves from one location to another (during migration). The main difference between these models and our model is that we

examine how a single cell senses the local substrate rigidity difference within the single cell domain. Therefore, our model can provide a more direct interpretation on how the cell sense the rigidity gradient.

In their original paper [1], Lo et al. proposed a two-part theory for the detection of the spatial gradient of the substrate rigidity as follows. In the first part of their theory, the cytoskeleton-focal adhesion-substrate linkages are considered as elastic springs (with spring constant k for the same amount of elastic energy input U from the active actomyosin contraction) to pull these springs, the spring force F enerated is larger at the stiffer region of the substrate underneath the cell (Because $U = \frac{F^2}{2k} \rightarrow F = \sqrt{2kU}$

thus for the same U larger k results in larger F In the second part the theory, the stronger force leads to a higher level of activation of force-sensitive proteins through conformational changes, which in turn leads to migration-related cellular responses such as upregulation of lamellipodia extension. The second part of the theory is referred to as mechanotransduction [27] in the literature. This two-part theory is directly supported by other experimental observations. For example, in a work by Breckenridge et al. [14], traction stress under a circular cell crossing step-rigidity boundary were measured using elastomeric micropost arrays. They found that the traction stress is higher on the stiffer half of the circular island (see Fig. 1b), which supports the first part of the theory. In another work [15], the authors found lamellipodia grow preferentially from the corners of square cells (see Fig. 1c). The corners of convex polygonal shapes are known to be the spots where high traction stress is generated when the cell contracts [28]. Together these findings support the

second part of the durotaxis theory that larger focal adhesion force leads to more lamellipodia extensions.

In this work, we are concerned with the first part of the theory: how exactly is the larger focal adhesion force generated in the part of the cell adhering to the stiffer region of the substrate? The assumption of Lo et al. that the same energy is provided for pulling is not without pitfalls, since it is not straightforward as how the generation of the same mechanical energy is ensured at the different sub-regions of the cell by the cell's active contractile apparatus. Another (and easier) approach to calculate the force is to consider the static equilibrium of the cell. The migrating speed of fibroblast cells is very slow ($\sim 1 \mu\text{m}/\text{min}$), considering the stress fibers are in a state of isometric tension, thus the cell at any time instant can be considered to be in a quasi-static equilibrium. Therefore, the static equilibrium holds for the whole mechanical system composed of the cell and the elastic substrate.

Using the method of static equilibrium, a simple generic model based on active matter theory has been devised by Marcq et al. [29], in which the cytoskeleton was modeled as two parallel elements (one passive spring and one active contractile element), and the 1D cell connects to the substrate springs only at the two ends (see Fig. 2a). Their model is sufficient to explain the experimental findings [17], [30] where the magnitude of the traction stress increases with the substrate rigidity. However, it cannot explain the rigidity gradient sensing (i.e., different traction stress at the two ends of the same cell): the static equilibrium implies that the adhesion forces

at the two ends of the cell should be the same, regardless of disparate substrate-spring stiffness. This is the paradox that was raised in a review by [31].

The assumption that the 1D cell only adheres to the substrate at the two ends oversimplifies the problem. In fact, by dropping this assumption, the abovementioned paradox can be resolved. Considering that the cell adheres to the substrate in the whole cell domain, in the present study, we show that the static equilibrium of the cell is sufficient to yield the rigidity gradient-dependent traction force distribution. The remainder of the paper is organized as follows. We first present the simple elasticity model for 1D and 2D cell adhering to an elastic substrate. For the 1D cell, we will derive analytical solutions and present results from the parametric studies. For the 2D cell, we will use the finite element method (FEM) to numerically solve the equilibrium equations. We then compare the modeling results with the three experimental observations listed in Fig. 1.

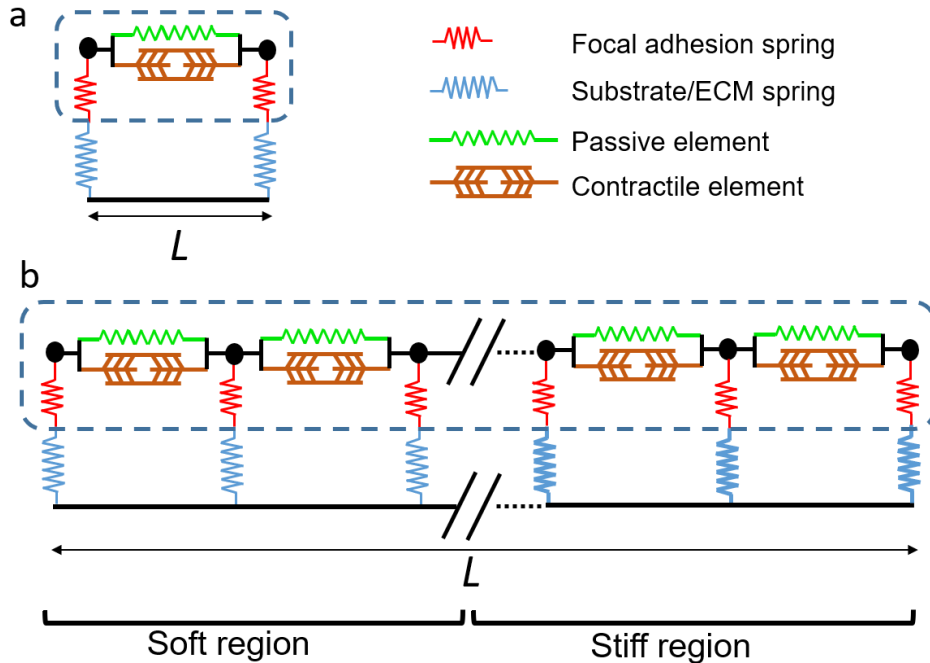


Figure 2. (a) Schematic representation of a single-cell model by Marcq et al. [29], where the cell adheres to the substrate only at the two ends. (b) Schematic representation of our single-cell model where the cell adheres to the substrate in the whole cell domain. The left half of the cell adhere to a soft region, while the right half of the cell adheres to a stiff region of the substrate. The cytoskeleton is composed of a passive spring and an active contractile element. Note that the FA and substrate springs, although drawn in a vertical direction, resist displacement in the horizontal direction in the 1D and 2D model.

Model description

1D Model

We first present a 1D model of a cell adhering to an elastic substrate. As shown in Fig. 2b, the cytoskeleton of the cell is modelled a 1D strip of length L adhering to the

substrate through the focal adhesions. The focal adhesions and the substrate are treated as linear springs of stiffness k_{FA} and k_{ECM} respectively. Note that k_{FA} and k_{ECM} denotes the stiffness of continuum springs so they are in units of stress per unit length, instead of force per unit length. Because the substrate is modeled as isolated springs (i.e., elastic interaction within the substrate is neglected), the substrate considered in our model can be thought as the elastomeric micropost arrays [14], rather than a continuum elastic substrate. The active actomyosin contraction shortens the 1D cell and the shortening is resisted by the passive component of the cytoskeleton and the substrate (see the schematic in Fig. 2b).

Constitutive relations of the cytoskeleton have been previously studied intensively. Time-dependent constitutive relations based on Hill's law of muscle contraction have been devised previously to capture the dynamic process of actomyosin contraction, such as for stress fibers [13], [17], [32] or for myofibrils [33], [34]. In this work, for simplicity, the final state of the dynamic models when contraction stress reaches isometric tension and strain rate becomes zero is considered, which yields a time-independent constitutive relation for the 1D cytoskeleton:

$$\sigma_x = E\varepsilon_x + \sigma_c \quad (1)$$

where σ_x is the overall cytoskeleton stress, E is the Young's modulus of the passive component of the cytoskeleton, σ_c is the isometric tension due to the active actomyosin contraction, $\varepsilon_x = \frac{\partial u_x}{\partial x}$ is the strain, u_x is the displacement along the axis of the 1D cell (i.e., x -axis).

The static equilibrium equation of the 1D cell is

$$h \frac{\partial \sigma_x}{\partial x} - T_x = 0 \quad (2)$$

where h is the thickness of the cell and is assumed to be a constant for simplicity, T_x is the traction stress exerted on the substrate by the cell. Because the focal adhesion is connected to the substrate spring in series, T_x is also the stress experienced by the focal adhesion. Therefore, we here use the phrases “focal adhesion stress” and “traction stress” interchangeably in this paper. Traction stress T_x can be calculated as

$$T_x = k_{CS} u_x \quad (3)$$

where k_{CS} is the equivalent spring constant of the cell-substrate linkage composed of the focal adhesion spring and the substrate spring, as illustrated in Fig. 2b. Because the two springs are in series, we have

$$k_{CS} = (k_{FA} k_{ECM}) / (k_{FA} + k_{ECM}) \quad (4)$$

To model the rigidity gradient, we define step changes in substrate rigidity by

$$k_{ECM} = \begin{cases} k_s, & x < 0 \\ \alpha k_s, & x > 0 \end{cases} \quad (5)$$

where α defines the ratio of rigidities of the two regions, which can be regarded as the gradient strength. Without loss of generality, the left half (i.e., $x < 0$) is considered to be softer than the right half (i.e., $x > 0$). Therefore, $\alpha \geq 1$ is imposed in our parametric studies. The stress-free boundary condition applies at the two ends: $\sigma_x(x = \pm L/2) = 0$ where L is the length of the 1D cell. The stress continuity condition at the interface between the stiff and soft regions is $\sigma_x(x = 0^-) = \sigma_x(x = 0^+)$. Equations (1)-(5), along with the boundary and interface conditions, can be solved analytically for the displacement u_x , stress σ_x and traction stress T_x .

2D Model

To apply the model to cells cultured on 2D surface of elastic substrate, we extend the 1D model to the 2D. For the 2D model, Eq. (1)-(3) become

$$\sigma_{ij} = 2Ge_{ij} + K\varepsilon_{kk}\delta_{ij} + \sigma_c\delta_{ij}$$

$$h\sigma_{ij,j} - T_i = 0$$

$$T_i = k_{cs}u_i$$

where the indicial notation is used, summation over repeated indices is adopted, σ_{ij} , e_{ij} , and ε_{ij} are stress tensor, deviatoric strain tensor, strain tensor, respectively, G and K are shear and bulk moduli of the cytoskeleton. the substrate rigidity gradient is modeled by defining k_{ECM} as a function of Cartesian coordinates (x, y) . The finite element method (FEM) [35] is used to numerically solve the differential equations of the 2D model, where 3-node triangle element is used for the spatial discretization.

Results

1D cell, when $\alpha = 1$

When the gradient strength parameter $\alpha = 1$, meaning uniform rigidity underneath the cell, the 1D model can be readily solved for the displacement u_x and traction T_x as follows. Using the strain-displacement and constitutive relations, Eq. (2) can be rewritten as an linear second-order differential equation: $hEu_{x,xx} - k_{cs}u_x = 0$. By

defining $\beta = \sqrt{\frac{k_{cs}}{Eh}}$, the solution can be written as, $u_x = ae^{\beta x} + be^{-\beta x}$ Imposing the

stress-free boundary condition at two ends (i.e., $\sigma_x(x = \pm L/2) = 0$) and, the two

unknown coefficients a and b are determined as: $a = -b = -\frac{\sigma_c}{E\beta} \frac{\gamma}{\gamma^2 + 1}$, where

$\gamma = e^{\frac{\beta L}{2}}$, Traction stress can be found using Eq. (3) as a function of x is:

$T_x(x) = -k_{cs} \frac{\sigma_c}{E\beta} \frac{\gamma}{1 + \gamma^2} (e^{\beta x} + e^{-\beta x})$. The magnitude of $T_x(x)$ maximizes at the two

ends of the cell (i.e., $x = \pm L/2$). Denoting the magnitude of traction stress located at

the two ends of the cell by T_{END} we have

$$T_{\text{END}} = k_{cs} \frac{\sigma_c}{E\beta} \frac{1 - \gamma^2}{1 + \gamma^2} \quad (6)$$

where k_{cs} is given in Eq. (4). Figure 3a plots T_{END} as a function of k_{ECM} which shows that the traction stress reaches a plateau when $k_{ECM} \rightarrow \infty$ which implies there is a saturation value of traction stress or force at large substrate rigidity. This result has been previously shown in experiments and models [17], [29], [30] Mathematically, this is simply because $k_{cs} \rightarrow k_{FA}$ when $k_{ECM} \rightarrow \infty$. Mechanically, this is because two springs in series is softer than any of the two springs. Therefore, when the substrate becomes rigid, the spring stiffness of the cell-substrate linkage becomes equal to the focal adhesion spring.

1D cell, when $\alpha > 1$

When $\alpha > 1$, a step change of rigidity is present underneath the single cell (the left half is always softer than the right half). The analytical solution can be derived similar to the case of $\alpha = 1$. Figure 3b and 3c show the solutions of traction stress T_x and cytoskeletal stress σ_x , respectively. For the traction stress, positive sign means

rightward pulling and negative sign means leftward pulling. Clearly, the traction stress magnitude is maximal at the cell edge on the stiff region (i.e., at the position $x/L = 1/2$). With continuous adhesion to the substrate in the whole cell domain, traction stress is redistributed so that on the stiffer side the traction stress is within a shorter range but higher magnitude on average. On average, the higher cytoskeleton stress σ_x is generated in the stiff region compared to the soft region. Note that traction stress is discontinuous at the interface (i.e., $x=0$). This is simply because the substrate rigidity is assumed to be discontinuous at the interface in our model (see Eq. 5, there is a step change of rigidity across $x=0$). If we assumed a linear-varying rigidity gradient, the traction stress would be continuous.

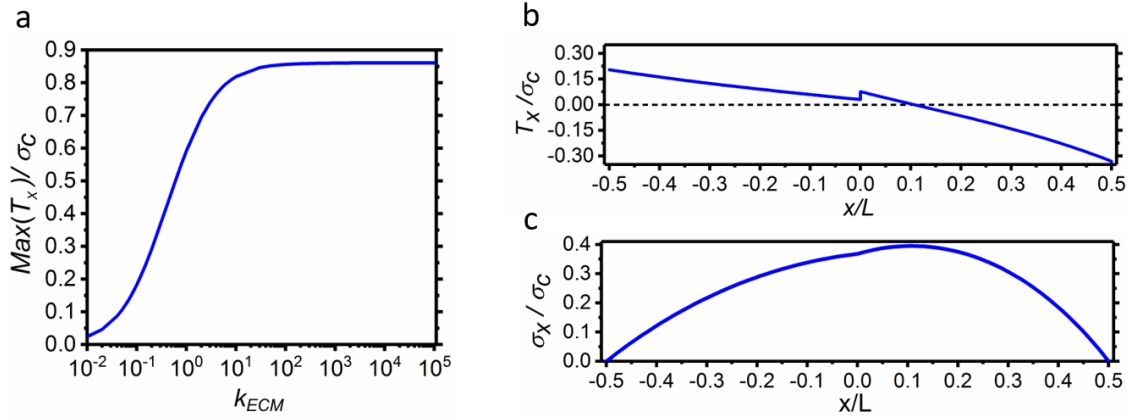


Figure 3. (a) Traction stress (scaled by σ_c) reaches a plateau at large substrate rigidity (in units of kPa/ μm). (b) Analytical solution of traction stress T_x . (c) Analytical solution of cytoskeletal stress σ_x . Parameter values used: $L = 20 \mu\text{m}$, $k_{FA}=1$ kPa/ μm , $k_s=0.1$ kPa/ μm , $h=3 \mu\text{m}$, $\sigma_c=4$ kPa, $\alpha = 3$, and $E=4$ kPa. These

parameter values are used for the remainder of the paper unless specifically mentioned.

These results imply that the static equilibrium alone can account for dependence of the traction stress on the rigidity gradient of the substrate, which is the first part of the rigidity-gradient sensing theory by Lo et al. mentioned previously. With the onset of different forces in focal adhesion and cytoskeleton, the positive feedbacks between the traction stress and focal adhesion maturation and between the cytoskeleton tension and the stress fiber formation can further amplify the differences of these forces, and eventually result into disparate cellular responses through mechanotransduction pathways.

Parametric studies were conducted to ascertain the sensitivity of the modeling results to the parameter values. We define the difference between the traction stresses at the left and right ends of the 1D cell as $\Delta T_x = |T_x(L/2)| - |T_x(-L/2)|$ where $||$ denotes the absolute value. Quantity ΔT_x represents the difference between the traction stresses on the soft and stiff regions of the substrate. Figure 4 plots the ΔT_x as a function of α for different values of E and k_s . In both Fig. 4a and 4b, we see that the traction stress difference increases with α which implies that the gradient strength play an important role in durotaxis [36], [37]. In Fig. 4a, we can see that ΔT_x increases as E decreases, meaning softer the passive component of the cytoskeleton, larger difference of traction stress is produced. When the passive component of the

cytoskeleton becomes stiffer, less contractile force is transmitted to the focal adhesion and consequently weaker dependence of focal adhesion stress on the substrate rigidity. In Fig. 4b, we can see that the ratio between the relative difference of traction stress between the soft and stiff regions (i.e., $\Delta T_x/T_{\max}$, where $T_{\max}=T_x(L/2)$) increases with decreasing substrate rigidity k_s which implies that if the mechanotransduction process detects the relative difference of traction stress, then softer substrate promotes durotaxis.

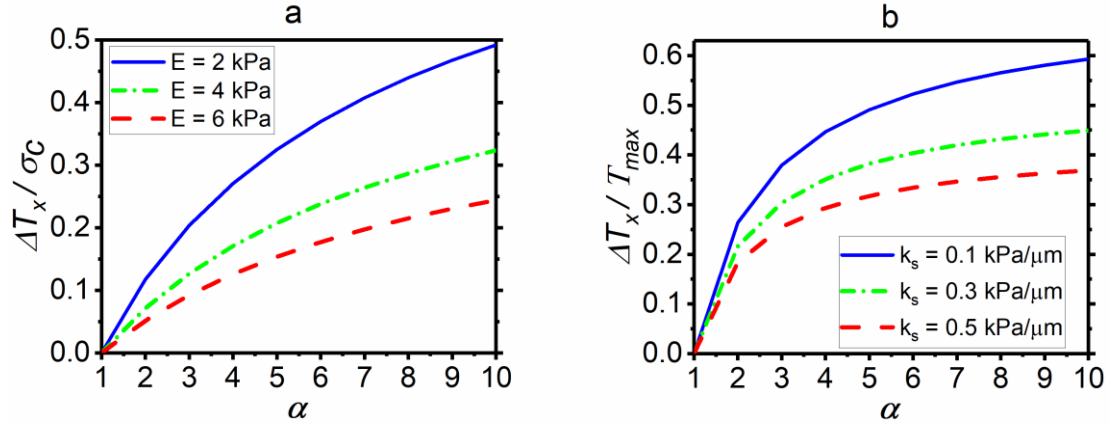


Figure 4. (a) Traction stress difference ΔT_x as a function of α for different values of E when $k_s=0.1$ kPa/ μm . (b) $\Delta T_x/T_{\max}$ as a function of α for different values of k_s when $E=2$ kPa.

Computational results for 2D cells

First, we show in Fig. 5a the FEM simulation results from the 2D cell model for a circular cell crossing a step-rigidity boundary (i.e., the upper half of the cell adheres to soft micropost arrays, the lower half of the cell adheres to stiff micropost arrays). As shown in Fig. 5a, the traction stress is higher on the perimeter of the cell, and it is

higher on the lower half (stiff substrate) compared to the upper half (soft substrate). The displacement is slightly higher on the upper half than the lower half. Our modeling results in Fig. 5a are in good agreement with in the experimental results [14] shown in Fig. 1b (if we neglect the random noise in the experiment). Therefore, both the experiment and our model show that the cytoskeleton contraction in the single cell generates higher traction stress on the stiffer region of the substrate underneath the cell.

Second, we show in Fig. 5b the model prediction of traction stress for the square cell. The traction stress concentrates to the edge of the square cell, and maximizes at the corners. This modeling result is correlated with the experimental data by [7], [15] shown in Fig. 1c where the lamellipodia extensions were localized to the corners of square-shaped cells. This correlation supports the durotaxis theory proposed by [1]: larger focal adhesion forces at the corners of the square cell are converted into protrusion signals via molecular mechanisms of mechanotransduction, which eventually lead to stronger lamellipodia extension. In the case of durotaxis, higher traction stresses are in the rigid side of the substrate and essentially the protrusion signals will be amplified in the rigid side rather than in the soft side.

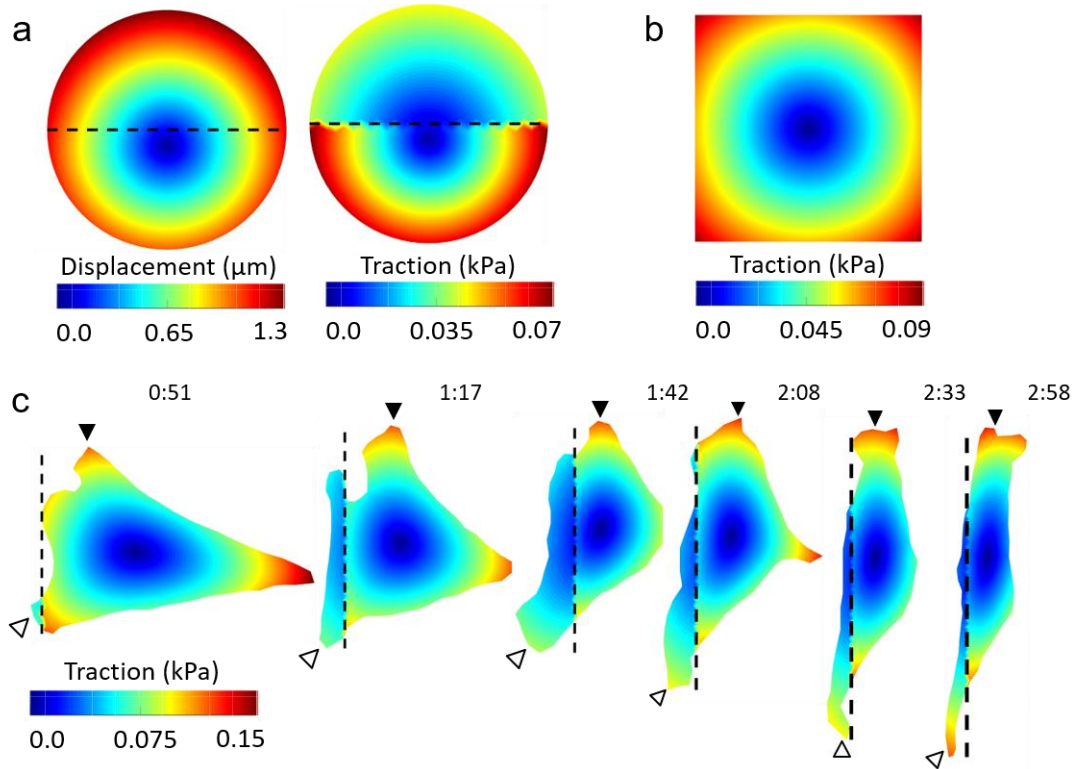


Figure 5. Finite element model predictions for 2D cells. (a) Displacement and traction stress of a circular cell crossing a step-rigidity boundary. (b) Traction stress for the square cell. (c) Traction stress distributions of the cell shown in Fig. 1a at the sequential time instants. (Parameter values used: $G=2.3$ kPa, $K=5$ kPa, cell area is $500 \mu\text{m}^2$, other parameters are the same as 1D analytical model given in Fig. 3)

We then apply the 2D model to Lo et al.'s experiment (Fig. 1a) to calculate the traction stress distribution. A vertical line is picked (approximately based on the brightness change in the image) in Fig. 1a to be the interface between the soft and stiff sides of the substrate. Figure 5c shows the traction stress distributions corresponding to the experimental images of Fig. 1a at the different time instants. One can see that the traction stress for the lamellipodia on the rigid side (solid arrowhead) is larger than that of the lamellipodia on the soft side (hollow arrowhead). If the larger force is

converted into more protrusion signal, the lamellipodia on the right side (solid arrowhead) will become the dominant one, which eventually leads to the turning of the cell at the step-rigidity boundary. Note that the highest traction stress spot at the tail of the cell at the beginning (see Fig. 5c) does not result in a leading head is probably because the memory (in the molecular constitutes) of the head-to-tail polarization [38], i.e., the new head will most likely to form near the original head.

Conclusions

In this work, we use a simple elasticity mechanics model to predict the traction stress (i.e., focal adhesion stress) for single adherent cells on the elastic substrate with rigidity gradient. The model predicts larger traction stress (i.e., larger focal adhesion stress because the traction stress is equal to the force experienced by the focal adhesion) on stiffer region of the substrate underneath a single cell. This minimal mechanics model provides a plausible answer for the first part of the durotaxis theory proposed by Lo et al. [1]: how exactly is the larger focal adhesion force generated in the part of the cell adhering to the stiffer region of the substrate? We found that the principle of static equilibrium alone provides a mechanistic explanation to this question. We think our model has resolved the paradox that was raised in a review by [31], which states that a static model cannot explain the rigidity sensing of a cell. Our model can be incorporated in more sophisticated mechanobiochemical models to address complex problems in mechanobiology and bioengineering.

Acknowledgments

H.Y. acknowledge funding support from the ASME Haythornthwaite Research Initiation Grant Award. X.Y. acknowledges the Thousand Youth Talent Plan Funds of China.

Compliance with ethical standards

Conflicts of interest

The authors declare that they do not have any conflict of interest.

References

- [1] C. M. Lo, H. B. Wang, M. Dembo, and Y.-L. Wang, “Cell movement is guided by the rigidity of the substrate,” *Biophys. J.*, vol. 79, pp. 144–152, 2000.
- [2] P. Uttayarat, G. K. Toworfe, F. Dietrich, P. I. Leikes, and R. J. Composto, “Topographic guidance of endothelial cells on silicone surfaces with micro- to nanogrooves: Orientation of actin filaments and focal adhesions,” *J. Biomed. Mater. Res. Part A*, vol. 75A, no. 3, pp. 668–680, 2005.
- [3] J. S. Harunaga and K. M. Yamada, “Cell-matrix adhesions in 3D,” *Matrix Biol.*, vol. 30, no. 7–8, pp. 363–368, 2011.
- [4] S. Li *et al.*, “The role of the dynamics of focal adhesion kinase in the mechanotaxis of endothelial cells,” *Proc. Natl. Acad. Sci. U. S. A.*, vol. 99, no. 6, pp. 3546–3551, 2002.
- [5] W. J. Polacheck, A. E. German, A. Mammoto, D. E. Ingber, and R. D. Kamm, “Mechanotransduction of fluid stresses governs 3D cell migration,” *Proc. Natl. Acad. Sci. U. S. A.*, vol. 111, no. 7, pp. 2447–52, 2014.
- [6] C. S. Chen, J. Tan, and J. Tien, “MECHANOTRANSDUCTION AT CELL-

- MATRIX AND CELL-CELL CONTACTS,” *Annu. Rev. Biomed. Eng.*, vol. 6, no. 1, pp. 275–302, 2004.
- [7] K. K. Parker *et al.*, “Directional control of lamellipodia extension by constraining cell shape and orienting cell tractional forces,” *Faseb J*, vol. 16, no. 10, pp. 1195–1204, 2002.
- [8] C. M. Nelson *et al.*, “Emergent patterns of growth controlled by multicellular form and mechanics,” *Proc. Natl. Acad. Sci. U. S. A.*, vol. 102, no. 33, pp. 11594–11599, 2005.
- [9] A. J. Engler, S. Sen, H. L. Sweeney, and D. E. Discher, “Matrix elasticity directs stem cell lineage specification,” *Cell*, vol. 126, no. 4, pp. 677–689, 2006.
- [10] V. Vogel and M. Sheetz, “Local force and geometry sensing regulate cell functions,” *Nat Rev Mol Cell Biol*, vol. 7, no. 4, pp. 265–275, 2006.
- [11] H. Yuan and H. Gao, “On the mechanics of integrin clustering during cell-substrate adhesion,” *Acta Mech. Solida Sin.*, vol. 25, no. 5, pp. 467–472, Oct. 2012.
- [12] H. Gao, J. Qian, and B. Chen, “Probing mechanical principles of focal contacts in cell–matrix adhesion with a coupled stochastic–elastic modelling framework,” *Journal of the Royal Society Interface*, vol. 8, no. 62. pp. 1217–1232, Sep-2011.
- [13] C. Borau, R. D. Kamm, and J. M. García-Aznar, “A time-dependent phenomenological model for cell mechano-sensing,” *Biomech. Model. Mechanobiol.*, vol. 13, no. 2, pp. 451–462, 2014.
- [14] M. T. Breckenridge, R. A. Desai, M. T. Yang, J. Fu, and C. S. Chen,

- “Substrates with engineered step changes in rigidity induce traction force polarity and durotaxis,” *Cell. Mol. Bioeng.*, vol. 7, no. 1, pp. 26–34, Mar. 2014.
- [15] A. Brock *et al.*, “Geometric determinants of directional cell motility revealed using microcontact printing,” *Langmuir*, vol. 19, no. 5, pp. 1611–1617, 2003.
- [16] H. B. Wang, M. Dembo, S. K. Hanks, and Y. Wang, “Focal adhesion kinase is involved in mechanosensing during fibroblast migration.,” *Proc. Natl. Acad. Sci. U. S. A.*, vol. 98, no. 20, pp. 11295–300, 2001.
- [17] D. Mitrossilis *et al.*, “Single-cell response to stiffness exhibits muscle-like behavior,” *Proc. Natl. Acad. Sci.*, vol. 106, no. 43, pp. 18243–18248, 2009.
- [18] S. V. Plotnikov, A. M. Pasapera, B. Sabass, and C. M. Waterman, “Force fluctuations within focal adhesions mediate ECM-rigidity sensing to guide directed cell migration,” *Cell*, vol. 151, no. 7, pp. 1513–1527, 2012.
- [19] S. Wong, W.-H. Guo, and Y.-L. Wang, “Fibroblasts probe substrate rigidity with filopodia extensions before occupying an area,” *Proc. Natl. Acad. Sci.*, vol. 111, no. 48, pp. 17176–17181, 2014.
- [20] P. Moreo, J. M. García-Aznar, and M. Doblaré, “Modeling mechanosensing and its effect on the migration and proliferation of adherent cells,” *Acta Biomater.*, vol. 4, no. 3, pp. 613–621, 2008.
- [21] C. Borau, R. D. Kamm, and J. M. García-Aznar, “Mechano-sensing and cell migration: A 3D model approach,” *Phys. Biol.*, vol. 8, no. 6, 2011.
- [22] A. Zemel, F. Rehfeldt, A. E. X. Brown, D. E. Discher, and S. A. Safran, “Optimal matrix rigidity for stress-fibre polarization in stem cells,” *Nat Phys*, vol. 6, no. 6, pp. 468–473, 2010.

- [23] A. Zemel, F. Rehfeldt, A. E. X. Brown, D. E. Discher, and S. A. Safran, “Cell shape, spreading symmetry, and the polarization of stress-fibers in cells,” *J. Phys. Condens. Matter*, vol. 22, no. 19, p. 194110, 2010.
- [24] O. Cohen and S. A. Safran, “Elastic interactions synchronize beating in cardiomyocytes,” *Soft Matter*, vol. 12, no. 28, pp. 6088–6095, 2016.
- [25] G. Yu, J. Feng, H. Man, and H. Levine, “Phenomenological modeling of durotaxis,” *Phys. Rev. E*, vol. 96, no. 1, pp. 1–6, 2017.
- [26] R. Allena, M. Scianna, and L. Preziosi, “A Cellular Potts Model of single cell migration in presence of durotaxis,” *Math. Biosci.*, vol. 275, pp. 57–70, May 2016.
- [27] C. S. Chen, “Mechanotransduction - a field pulling together?,” *J. Cell Sci.*, vol. 121, no. 20, pp. 3285–3292, 2008.
- [28] H. Yuan, B. Marzban, and K. K. Parker, “Myofibrils in Cardiomyocytes Tend to Assemble Along the Maximal Principle Stress Directions,” *J. Biomech. Eng.*, vol. 139, no. 12, 2017.
- [29] P. Marcq, N. Yoshinaga, and J. Prost, “Rigidity sensing explained by active matter theory,” *Biophys. J.*, vol. 101, no. 6, pp. 26–29, 2011.
- [30] M. Ghibaudo *et al.*, “Traction forces and rigidity sensing regulate cell functions,” *Soft Matter*, vol. 4, no. 9, pp. 1836–1843, 2008.
- [31] G. Danuser, J. Allard, and A. Mogilner, “Mathematical modeling of eukaryotic cell migration: insights beyond experiments,” *Annu Rev Cell Dev Biol*, vol. 29, pp. 501–528, 2013.
- [32] V. S. Deshpande, R. M. McMeeking, and A. G. Evans, “A bio-chemo-

- mechanical model for cell contractility,” *Proc. Natl. Acad. Sci. U. S. A.*, vol. 103, no. 38, pp. 14015–14020, 2006.
- [33] M. L. McCain, H. Yuan, F. S. Pasqualini, P. H. Campbell, and K. K. Parker, “Matrix elasticity regulates the optimal cardiac myocyte shape for contractility,” *Am. J. Physiol. Heart Circ. Physiol.*, vol. 306, no. 11, pp. H1525–39, Jun. 2014.
- [34] Y. Aratyn-Schaus *et al.*, “Coupling primary and stem cell–derived cardiomyocytes in an in vitro model of cardiac cell therapy,” *J. Cell Biol.*, vol. February 8, 2016.
- [35] O. C. Zienkiewicz, R. L. Taylor, and J. Z. Zhu, *The Finite Element Method: its Basis and Fundamentals*. 2005.
- [36] B. C. Isenberg, P. A. Dimilla, M. Walker, S. Kim, and J. Y. Wong, “Vascular smooth muscle cell durotaxis depends on substrate stiffness gradient strength,” *Biophys. J.*, vol. 97, no. 5, pp. 1313–1322, Sep. 2009.
- [37] L. G. Vincent, Y. S. Choi, B. Alonso-Latorre, J. C. del Alamo, and A. J. Engler, “Mesenchymal stem cell durotaxis depends on substrate stiffness gradient strength,” *Biotechnol. J.*, vol. 8, no. 4, pp. 472–484, Apr. 2013.
- [38] H. V. Prentice-Mott *et al.*, “Directional memory arises from long-lived cytoskeletal asymmetries in polarized chemotactic cells,” *Proc. Natl. Acad. Sci.*, vol. 113, no. 5, p. 201513289, 2016.
- [39] P. Devreotes and A. R. Horwitz, “Signaling networks that regulate cell migration,” *Cold Spring Harb Perspect Biol*, vol. 7, no. 8, p. a005959, 2015.
- [40] J. Satulovsky, R. Lui, and Y. Wang, “Exploring the Control Circuit of Cell

- Migration by Mathematical Modeling,” *Biophys. J.*, vol. 94, no. 9, pp. 3671–3683, 2008.
- [41] A. J. Ridley *et al.*, “Cell migration: integrating signals from front to back,” *Science*, vol. 302, no. 5651, pp. 1704–9, Dec. 2003.
- [42] M. D. Onsum and C. V Rao, “Calling heads from tails : the role of mathematical modeling in understanding cell polarization,” pp. 74–81, 2009.
- [43] R. Wedlich-Soldner, S. Altschuler, L. Wu, and R. Li, “Spontaneous cell polarization through actomyosin-based delivery of the Cdc42 GTPase,” *Science (80-.)*, vol. 299, no. 5610, pp. 1231–1235, 2003.
- [44] A. F. M. Marée, A. Jilkine, A. Dawes, V. A. Grieneisen, and L. Edelstein-Keshet, *Polarization and movement of keratocytes: A multiscale modelling approach*, vol. 68, no. 5. 2006.
- [45] P. a. Iglesias and P. N. Devreotes, “Biased excitable networks: How cells direct motion in response to gradients,” *Curr. Opin. Cell Biol.*, vol. 24, no. 2, pp. 245–253, 2012.
- [46] Y. Xiong, C.-H. Huang, P. A. Iglesias, and P. N. Devreotes, “Cells navigate with a local-excitation, global-inhibition-biased excitable network,” *Proc. Natl. Acad. Sci.*, vol. 107, no. 40, pp. 17079–17086, 2010.
- [47] M. P. Sheetz and J. Dai, “Modulation of membrane dynamics and cell motility by membrane tension,” *Trends Cell Biol.*, vol. 6, no. 3, pp. 85–89, 1996.
- [48] M. P. Sheetz, D. P. Felsenfeld, and C. G. Galbraith, “Cell migration : regulation of force on extracellular-matrix-integrin complexes,” *Trends Cell Biol.*, vol. 8, no. 97, pp. 51–54, 1998.

- [49] A. del Rio, R. Perez-jimenez, R. Liu, P. Roca-Cusachs, J. M. Fernandez, and M. P. Sheetz, “Stretching Single Talin Rod Molecules Activates Vinculin Binding,” *Science* (80-.), vol. 323, no. 5914, pp. 638–641, Jan. 2009.
- [50] B. Marzban, X. Yi, and H. Yuan, “A minimal mechanics model for mechanosensing of substrate rigidity gradient in durotaxis,” *Biomech. Model. Mechanobiol.*, Jan. 2018.
- [51] A. Rahman *et al.*, “Vinculin regulates directionality and cell polarity in two- and three-dimensional matrix and three-dimensional microtrack migration,” *Mol. Biol. Cell*, vol. 27, no. 9, pp. 1431–1441, 2016.
- [52] M. Yao *et al.*, “Force-dependent conformational switch of α -catenin controls vinculin binding,” *Nat. Commun.*, vol. 5, Jul. 2014.
- [53] F. Twiss and J. De Rooij, “Cadherin mechanotransduction in tissue remodeling,” *Cell. Mol. Life Sci.*, vol. 70, no. 21, pp. 4101–4116, 2013.
- [54] H. Yuan, B. Marzban, and K. K. Parker, “Myofibrils in Cardiomyocytes Tend to Assemble Along the Maximal Principle Stress Directions,” *J. Biomech. Eng.*, vol. 139, no. December 2017, pp. 1–8, 2017.
- [55] G. Forgacs and S. A. Newman, *Biological Physics of the Developing Embryo*. Cambridge: Cambridge University Press, 2005.
- [56] A. F. M. Marée, V. A. Grieneisen, and L. Edelstein-Keshet, “How cells integrate complex stimuli: The effect of feedback from phosphoinositides and cell shape on cell polarization and motility,” *PLoS Comput. Biol.*, vol. 8, no. 3, 2012.
- [57] S. J. Altschuler, S. B. Angenent, Y. Wang, and L. F. Wu, “On the spontaneous

emergence of cell polarity,” *Nature*, vol. 454, no. 7206, pp. 886–889, 2008.

- [58] H. Yuan, B. Marzban, and K. K. Parker, “Myofibrils in Cardiomyocytes Tend to Assemble Along the Maximal Principle Stress Directions,” *J Biomech Eng*, vol. doi: 10.11, 2017.

CHAPTER 3:

A contraction-reaction-diffusion model for cell migration: integrating biomechanics and biochemistry at the whole cell level

by

Bahador Marzban, Yubing Sun, Hongyan Yuan*

To be submitted in Biophysical Journal

*Corresponding Author:

Hongyan Yuan

Department of Mechanical, Industrial and Systems Engineering,

University of Rhode Island,

331A Pastore Hall, 51 Lower College Road, Kingston, RI

02881, USA

USA phone: +1-401-874- 2774

Email: hongyan_yuan@uri.edu

ABSTRACT

Cell migration is a fundamental biological process involved in tissue morphogenesis and cancer metastasis. To understand how cell migration works at the whole cell level, biomechanical and biophysical models have been developed but were mainly independent of each other. In this work, by integrating biomechanics and biochemistry of the cell, we developed a contraction-reaction-diffusion model for cell migration at the whole-cell scale. The mechanics of cytoskeleton contraction generates distributed forces for the cell to sense the mechanical properties of itself and its microenvironment. The mechanosensing is coupled with the reaction and diffusion of biomolecules in the cell to model the cell migration. The simulation results show that the model can simulate cell polarization (head-to-tail formation), the localization of protrusion signal to the corners of the square cell, and cytoskeleton asymmetry-dependent persistent migration. In addition, this dynamic model of cell migration can recapitulate durotaxis *in silicon* and simulate cellular morphogenesis. The single cell model can be extended to multicellular model for understanding microtissue formation.

Keywords: Cell migration, cytoskeletal contraction, durotaxis, virtual-cell simulation, reaction-diffusion

Introduction

Cell migration, an intriguing phenomenon involved in tissue formation and cancer metastasis, has long been the subject of intensive investigation in the fields of

biophysics and cell biology [1]. The machineries that drive migration, and the signaling networks that control the migration machineries have been studied intensively [2]. In vitro 2D cell migration experiments revealed that cells of different types, such as fibroblasts, keratocytes, and neurons, exhibit different migration/spreading behaviors [3]. On the other hand, different types of cells share some fundamental characteristics. In general, single cell migration can be described as a coordinated and integrated process of different modules (**Fig. 1**): cell polarization (i.e., front-and-rear formation), protrusion of lamellipodia/filopodia/lobopodia, invadopodia formation and proteolysis of surrounding ECM, formation of new adhesions in the front, releasing of aging adhesions at the rear, and cytoskeleton/membrane skeleton contraction to move the rear forward [2], [4].

Inspired by Turing's reaction-diffusion model of diffusive biochemical molecules, mathematical models were developed to study cell polarization [5], [6], and cell morphogenesis in migration [3], [7]. Particularly, the reaction and diffusion of intracellular signaling molecules have been interpreted as to form networks [8], [9]. Cells with this internal network system are able to spontaneously polarize and make persistent random walks in the absence of external cues [3], and to carry out directed movement when biased by external signal gradients (i.e., chemotaxis).

On the other hand, biomechanics has been shown to play a critical role in many biological functions such as cell motility [10]–[12]. It has been postulated that the mechanosensitive proteins change their conformations when stretched by mechanical forces, and the conformational changes open up hidden active sites for binding with other molecules, which in turn results in specific chemical reactions. For example,

stretching of talin protein resulting in the increased binding of vinculin to talin [13], which may be a molecular mechanism underlying the force-dependent focal adhesion maturation [14], [15], [16]. Similarly, stretching of α -catenin has been shown to induce enhanced vinculin binding in cell-cell adhesion [17], [18]. Mechanical forces also regulate the actomyosin stress fiber formation [19]. Therefore, mechanical and geometrical properties of cells and their microenvironments are not merely passive consequence of biochemistry. In steady, they are important regulators of biological processes such as cell migration.

Biochemical models based on reaction-diffusion equations lack the consideration of mechanotransduction thus cannot capture mechanosensing in cell migration. Biomechanics models lack consideration of biochemical signaling and thus fail to account for biochemical processes. A thorough understanding of cell migration will require the elucidation of how the mechanical and biochemical events are spatiotemporally integrated at the cellular scale. In this work, we develop a contraction-reaction-diffusion model for cell migration by integrating the mechanical force generation and reaction-diffusion of biochemical molecules at the whole-cell scale. Our overarching hypothesis is the following: the biomechanical and biochemical signals form mechanobiochemical feedback loops. Through the mechanobiochemical feedback loop, cell migration and cell shape can be regulated by a variety of mechanical cues, such as cell shape [20] and substrate rigidity gradient [21].

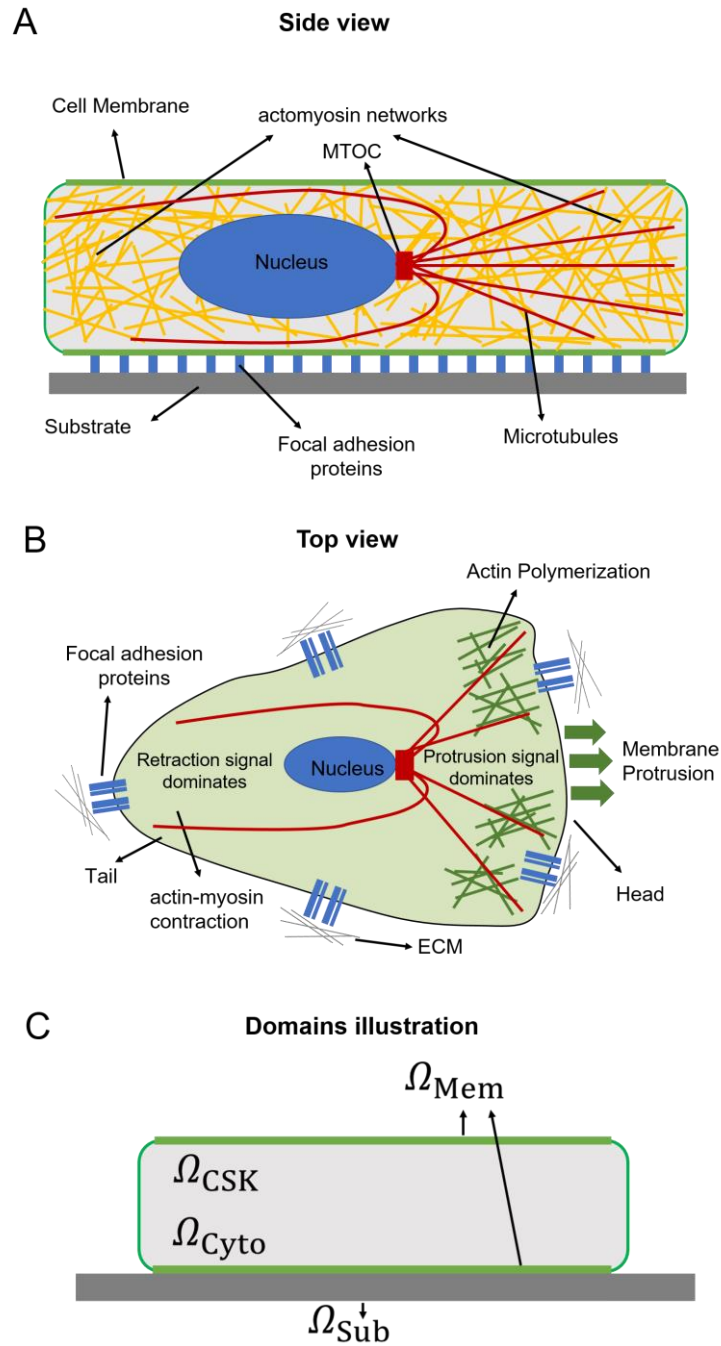


Figure 1. Schematic illustrations of cell migration on a 2D surface. A) Side view, B) Top view. C) Physical domains defined in the cell model.

Model Description

The present computational model is concerned with cells spreading and migrating on the surface of the substrate. Cells are modeled as a two-dimensional (2D) continuum, which reflects the flatness of the lamellipodia for cells cultured on 2D flat substrates. As illustrated in Fig. 1C, four physical domains are defined for the cell: cytoskeleton domain Ω_{CSK} , cytosol domain Ω_{Cyto} , membrane domain Ω_{Mem} , and substrate domain Ω_{Sub} . In the cell membrane domain Ω_{Mem} , reaction-diffusion equation of protrusion signaling molecules are formulated. In the cytosol domain Ω_{Cyto} , reaction-diffusion equation of retraction-related molecules are formulated. In the cytoskeleton domain Ω_{CSK} , solid mechanics equations are formulated, and the mechanical stresses in cytoskeleton are solved. Because 2D model of the cell is adopted, the physical domains Ω_{CSK} , Ω_{Cyto} , Ω_{Mem} , and Ω_{Sub} can be described by the same mathematical domain, denoted by Ω . The single-cell model is composed of five modules: cytoskeleton mechanics, reaction-diffusion of molecules, cytoskeleton asymmetry, protrusion and retraction of cell body, and cell-substrate interaction, which will be described below.

Cytoskeleton module

The elasticity model of the cytoskeleton

A rather simple mechanics model of cytoskeleton is adopted here. Because the migration of biological cells in their solid or fluid microenvironment is at the low Reynolds number [22], the inertia force can be neglected. At each time instant, the cell can be considered in a quasi-static equilibrium. The equilibrium equation of the

cytoskeleton in the domain Ω_{CSK} are written by using Cartesian tensor notation (summation over repeated indices is adopted hereinafter) as

$$h_c \sigma_{ij,j} - T_i = 0 \quad (1)$$

where σ_{ij} is the Cauchy stress tensor of the cytoskeleton (i and j takes values of 1 and 2 in 2D), h_c is the thickness of the cell, which is assumed to be uniform throughout the cell. Denoting A_c the area of the cell, the volume of the cell is calculated as

$$V_c = A_c h_c \quad (2)$$

The cell volume is assumed to be conserved in the present study, so h_c varies with time when the cell area changes. Here T_i is the traction stress exerted on the substrate by the cell. At the cell edge (denoted by Γ) where there is no cell-cell adhesion, the stress-free boundary condition holds: $\sigma_{ij} n_j = 0$, where n_j is the normal direction at the cell edge. In the present model, the cytoskeleton is composed of passive and active networks. For the sake of simplicity, a simple elastic constitutive relation is adopted,

$$\sigma_{ij} = 2G e_{ij} + K \varepsilon_{kk} \delta_{ij} + \Sigma_{ij} \quad (3)$$

where $\varepsilon_{ij} = \frac{1}{2}(u_{i,j} + u_{j,i})$ is the strain tensor, u_i is the displacement, $e_{ij} = \varepsilon_{ij} - \varepsilon_{kk}/3$ is the deviatoric strain tensor, G and K are shear and bulk modulus of the passive network, Σ_{ij} is the active isometric tensile stress (ITS) tensor from the active part of the cytoskeleton, which will be defined later in Eq. (6). Use of the small-strain Hooke's law in Eq. (3) for the large deformation that occurs during cell motility deserves some explanations here. In this model, when solving the elasticity problem for a migrating cell, at each time instant we treat the current configuration as the

stress-free state, and displacement u_i and strain ε_{ij} are measured from the current stress-stress configuration, rather than the reference state at an initial time of the whole migration process. Note that the displacement and strain concepts here are different than those in the conventional finite-strain elasticity theory. This is an ad hoc treatment based on the assumption that the dynamic bonds that forms the passive network of the cytoskeleton remodels fast enough to release the passive stress in the cytoskeleton. The traction stress is assumed to be linearly proportional to the “instantaneous” displacement u_i of the cell

$$T_i = k_{cs}u_i \quad (4)$$

where k_{cs} is the spring constant of the cell-substrate linkage that will be defined later in Eq. (18).

Stress-fiber structure tensor

To account for the anisotropic fiber formation, a previously defined mathematical model for myofibril orientation in cardiomyocytes is used [20]. A second-order tensor S_{ij} , referred to as the stress-fiber structure tensor, is defined and its time evolution is described by

$$\frac{dS_{ij}}{dt} = K_{on}^S \frac{1}{\sigma_t + \sigma_m} \sigma_{ij} H(\sigma_t) - K_{off}^S S_{ij} \quad (5)$$

where K_{on}^S and K_{off}^S are the stress fiber activation and deactivation rates, respectively. Here, σ_m is a model parameter, $\sigma_t = \sigma_{kk}/2$ is the cytoskeletal tension, $H(\)$ denotes Heaviside function and is defined as: $H(x)=1$ when $x > 0$ and $H(x)=0$ when $x \leq 0$. Denoting the maximal eigenvalue and the corresponding eigenvector of S_{ij} by λ_1 and m_i^1 , respectively, the ITS tensor Σ_{ij} is defined as

$$\Sigma_{ij} = (\sigma_{c0} + \sigma_{c1}\zeta)\delta_{ij} + \sigma_{cf}\lambda_1 m_i^1 m_j^1 \quad (6)$$

where σ_{c0} , σ_{c1} , and σ_{cf} denotes the baseline, retraction signal-associated, and stress fiber-associated contractility, ζ is the concentration of retraction signal that will be introduced below. The dyadic product of unit vector m_i^1 produces the tensor $m_i^1 m_j^1$, which has its only non-zero-principle-value principle direction along m_i^1 . This anisotropic cytoskeleton model has been used to explain the pattern formation of myofibrils in single cardiomyocytes [19].

Cell motility module

In this work, we adopt a similar modeling concept as Satulovsky et al. [3] where a few phenomenological variables are used to represent the concentration of various proteins involved in cell migration.

Reaction-diffusion of protrusion and retraction signals

Previous studies indicated that the active forms of protrusion and retraction signals are membrane-bound proteins [7], [23]. Two phenomenological variables ξ and ζ are defined in the physical domain of the membrane Ω_{Mem} to account for the area concentration of active form of protrusion (e.g., Rac, Cdc42) and retraction (e.g., ROCK) signals, respectively [3]. Here variables ξ and ζ are normalized by their saturation values respectively thus are in units of μm^{-2} and with the maximal value of $1 \mu\text{m}^{-2}$. Their time evolution equations are defined as

$$\frac{D\xi}{Dt} = D_\xi \Delta \xi + \left[\frac{K_0^\xi}{1+(\zeta/\zeta_0)^{n_1}} + K_T^\xi \left(\frac{T^{n_2}}{T^{n_2} + T_0^{n_2}} \right) \rho + K_M^\xi f_M \xi \right] (h_c \xi_i) - K_{\text{off}}^\xi \xi + \sqrt{R_\xi} G(t) \quad (7)$$

$$\frac{D\zeta}{Dt} = D_\zeta \Delta \zeta + \left[\frac{K_0^\zeta}{1+(\xi/\xi_0)^{n_3}} \right] (h_c \zeta_i) - K_{\text{off}}^\zeta \zeta + \sqrt{R_\zeta} G(t) \quad (8)$$

where $\frac{D}{\partial t}$ represents the material time derivative (the cytosol is assumed to be moved with the cytoskeleton, convection of cytosol is not considered here), $\Delta = \frac{\partial^2}{\partial x^2} + \frac{\partial^2}{\partial y^2}$ is the Laplace operator, D_ξ and D_ζ are the protrusion and retraction diffusion constants in the membrane, K_0^ξ , K_M^ξ , and K_T^ξ are the rate constants for the spontaneous, auto-activation, and stress-mediated protrusion signal activations, K_0^ζ is the spontaneous activation rate for retraction signal, K_{off}^ξ and K_{off}^ζ are the decay constants for the protrusion and retraction signals, respectively. Here, ξ_0 , ζ_0 , n_1 , n_2 , n_3 are model parameters describing the auto-inhibition relation between the protrusion and retraction signals, R_ξ and R_ζ denote strength of random noise for protrusion and retraction signals, respectively, $G(t)$ is a Gaussian random process of mean zero and variance unity and $\langle G(t)G(t') \rangle = \delta(t - t')$, ξ_i and ζ_i are the volume concentration of the inactive forms of protrusion and retraction signaling molecules in the cytosol, which are in units of μm^{-3} . The diffusion of inactive protrusion and retraction signaling molecules in the cytosol are considered much faster than in the membrane. To be simple, ξ_i and ζ_i are assumed to be uniform in the cytosol and are calculated by the following two equations, respectively,

$$h_c \xi_i = h_c \xi_a - \bar{\xi} \quad (9)$$

$$h_c \zeta_i = h_c \zeta_a - \bar{\zeta} \quad (10)$$

where ξ_a and ζ_a are model parameters denoting the total volume concentrations of both active and inactive forms for protrusion and retraction signals, respectively, $\bar{\xi}$ and $\bar{\zeta}$ are the spatial mean values of ξ and ζ , respectively. In Eq. (9), multiplying ξ_i by cell thickness h_c to convert a volume concentration to an area concentration is based

on the assumption that the cell is flat and the diffusion in the cell thickness direction is instantaneous.

Movement of the cell (i.e., protrusion and retraction)

The movement of the cell consists of the cell protrusion caused by the actin polymerization at the leading edge of the lamellipodia and the passive retraction as a result of active cytoskeleton contraction. A protrusion velocity \mathbf{v}^p is defined as a function of the protrusion signal at the cell edge Γ as

$$v_i^p = c_p H(\xi - \xi_p) H(A_{\max} - A_c) \rho \xi n_i \quad (11)$$

where model parameter c_p represent the intrinsic level of membrane protrusion speed, parameter ξ_p is the threshold of protrusion signal above which membrane protrusion occurs, parameter A_{\max} sets an upper limit of the cell area, n_i is the outward normal unit vector at the cell edge. The retraction velocity is assumed to be proportional to the instantaneous displacement u_i of the cytoskeleton as,

$$v_i^R = c_r u_i H(A_c - A_{\min}) \quad (12)$$

where c_r is a model parameter.

Cytoskeletal asymmetry

Experimental studies have revealed that the cell polarity (i.e., head-and-tail pattern) is maintained through the long-lived cytoskeletal asymmetries including microtubules [24]. To incorporate the cytoskeletal asymmetries in the model, a vector \mathbf{M} is defined to represent the polarity of the asymmetric cytoskeleton and its time evolution equation is defined as,

$$\frac{d\mathbf{M}}{dt} = K_M(\mathbf{M}_\xi - \mathbf{M}) \quad (13)$$

where K_M is a model parameter, vector \mathbf{M}_ξ is a vector defined based on the protrusion signal,

$$\mathbf{M}_\xi = \frac{m_c}{A_c} \oint_{\Gamma} \xi |\mathbf{r}_e|^2 \hat{\mathbf{r}}_e d\theta \quad (14)$$

Where m_c is a model parameter, $\hat{\mathbf{r}}_e = \mathbf{r}_e/|\mathbf{r}_e|$ is a unit vector and \mathbf{r}_e is the position vector of the edge points relative to the center of the cell, $|\mathbf{r}_e|$ is the length of \mathbf{r}_e , $d\theta$ is the differential angle corresponding to the differential arc length, where θ is the angle coordinate of the edge point in the polar coordinate system with the cell center as the origin. As implied by Eq. (13), in the steady-state ($d\mathbf{M}/dt=0$), the cytoskeleton asymmetry vector \mathbf{M} is equal to the vector \mathbf{M}_ξ . The cytoskeleton-asymmetry function $f_M(s)$ in Eq. (7) is defined with the angle θ_M of the vector \mathbf{M} as,

$$f_M(\theta) = \left((1 + \cos(\theta - \theta_M)) / 2 \right)^{n_M} \quad (15)$$

where n_M is a model parameter.

Cell-substrate interaction module

To incorporate the dynamic remodeling of focal adhesion, a phenomenological variable ρ is defined to describe the density distribution of focal adhesion-associated proteins (e.g., integrins, talins, vinculins, etc.). Variable ρ is normalized by the saturation value, thus ranges from zero (no integrin-mediated cell-substrate adhesion) to one (mature FAs). The time evolution of ρ is described by

$$\frac{D\rho}{dt} = \left[K_0^\rho + K_\xi^\rho \xi + K_T^\rho \left(\frac{T^{n_4}}{T^{n_4} + T_0^{n_4}} \right) \rho + K_M^\rho f_M \rho \right] \rho_i - K_{\text{off}}^\rho \rho + \sqrt{R_\rho} G(t), \quad (16)$$

where $K_0^\rho, K_M^\rho, K_\xi^\rho$, and K_T^ρ are the rate constants for the spontaneous, auto-activation, protrusion signal-dependent, and stress-mediated focal adhesion formation, respectively, K_{off}^ρ is a decay constant, T denotes the magnitude of the traction stress, T_0 and n_4 are model parameters, and R_ρ is the strength of random noise. Here the redistribution (e.g., via active transportation and passive diffusion) of unbound focal adhesion proteins is assumed to be faster than other time scale of focal adhesion formation, the unbound focal adhesion protein density ρ_i in the membrane is simply computed as

$$\rho_i = \rho_a - \bar{\rho} \quad (17)$$

where $\bar{\rho}$ is the mean value of ρ in the membrane domain, and ρ_a represents the average density of the total amount of bound and unbound focal adhesion proteins. Denoting k_{FA} and k_{ECM} the equivalent spring constants of the focal adhesion and the substrate, respectively, the spring constant of the cytoskeleton-substrate linkage is given as

$$k_{cs} = (k_{FA}k_{ECM})/(k_{FA} + k_{ECM}) \quad (18)$$

The mechanics of the cell is coupled to the dynamics of focal adhesion remodeling through the spring stiffness k_{FA} by the following relation

$$k_{FA} = k_{FA}^{max} \rho \quad (19)$$

where k_{FA}^{max} is the maximal stiffness when the focal adhesion density $\rho = 1 \mu\text{m}^{-2}$ (i.e., mature focal adhesion).

Numerical implementation of the model

The cell monolayer model is implemented in an in-house code using the finite element method, where Lagrangian mesh is adopted and 3-node triangle element is

used. In the simulations of the movement of the cell, the nodal spatial coordinates are updated based on Eq. (11) and Eq. (12). An auto mesh-generating algorithm based on Delaunay triangulation is utilized to perform re-meshing when mesh distortion occurs. Mesh transfer for the field variables is performed between the old and new mesh.

Mechanosensing at the whole-cell scale

As illustrated in Fig. 2, the coupling of different modules in our model are illustrated in Fig. 2. Starting from the lower right block, cell contraction generates mechanical stresses in the cell. These forces are converted into biochemical activities through mechanosensors, which in turn regulate the assembly/disassembly of macromolecular entities (lower left block) and the cell protrusion/retraction (upper left block). The macromolecular assembly/disassembly alter the structural, geometrical, and material properties of the cell, which, according to the continuum/structural mechanics theory, will subsequently change both the internal stress (cytoskeleton stress) and stress at the boundary (i.e., cell-matrix adhesion stress). Thus, mechanics of the cell, biochemical activities, and macromolecular assemblies are coupled through mechanobiochemical feedback loops.

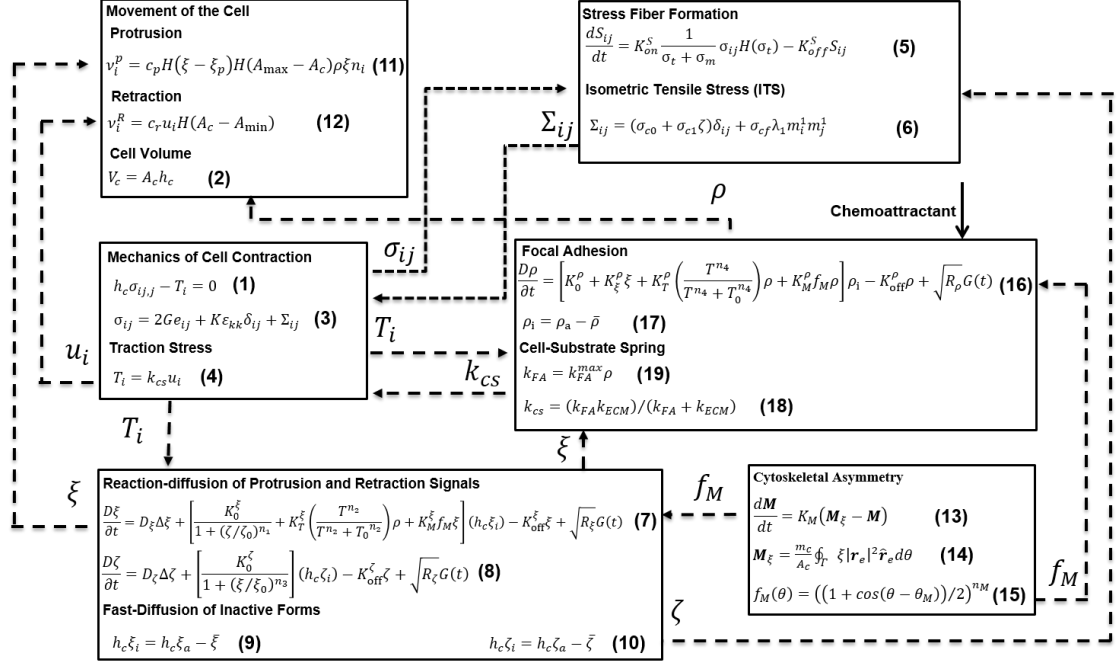


Figure 2. Block diagram for the model, note that numbers in parentheses are equation numbers.

Simulation results

Establishment of polarity of the cell with the reaction-diffusion submodel

Cell polarization (i.e., forming head and tail) is critical in cell migration to achieve directed movement. The spontaneous polarization has been thought as a pattern formation in reaction-diffusion systems [3], [23], [25]. We here define the system of equations consisting of Eq. (6)-(9), where K_T^ξ and K_M^ξ are set to be zero, as the reaction-diffusion submodel. In this reaction-diffusion submodel, which were previously proposed by Maree et al [7], the protrusion signal ξ and retraction signal ζ inhibit each other through the K_0^ξ and K_0^ζ terms, respectively. As studied by Maree et

al, this simple mutual-inhibition model can induce spontaneous polarization. Figure 3 shows the simulation result of the reaction-diffusion submodel. As shown in Fig. 3A (top row), starting with a randomly perturbed initial state, the protrusion signal ξ in a circular cell spontaneously polarizes, i.e., spatially separates into two zones: high and low regions. Because of the auto-inhibition, retraction signal distribution also polarizes.

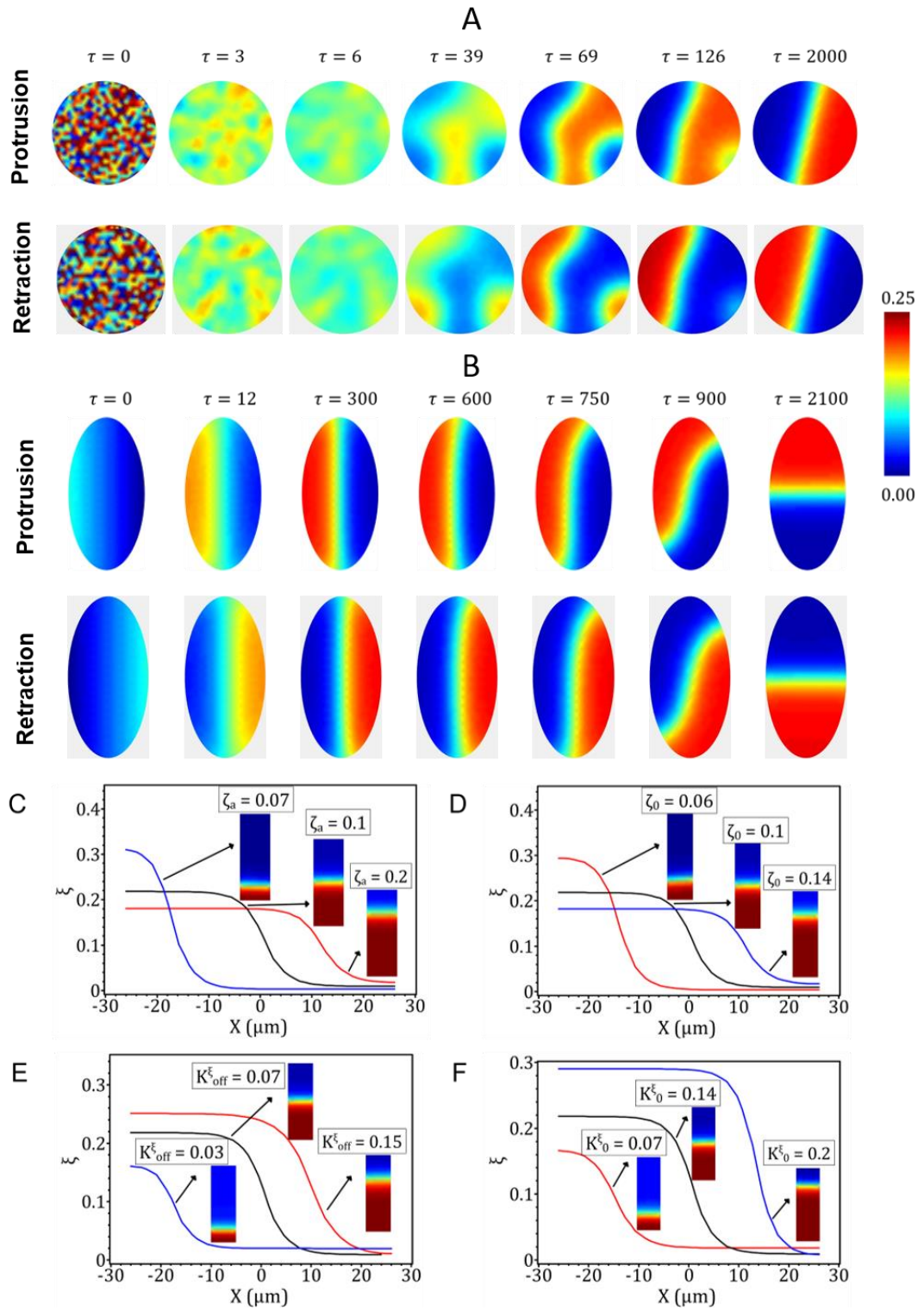


Figure 3. Establishment of polarity of the cell with the reaction-diffusion submodel. (A) In a circular cell, protrusion signal ξ polarizes spontaneously with random initial perturbation. (B) The effect of cell shape on the spatial patterns of protrusion signal in an elliptical cell. (C)-(F) Effect of modal parameters ζ_a , ζ_0 , K_0^ξ , and K_{off}^ξ on the steady-state distribution of protrusion signal ξ . Note that all the panels share the same color bar.

As previously showed by Maree et al. [23], the cell shape (i.e., the shape of the mathematical domain of the reaction-diffusion equations) has an important effect on the spatial patterns formed. They concluded that at the steady state, the length of the interface that separates the high and low regions is minimized. Our simulation results agree with their conclusion. As shown in Figure 3B, the interface in the elliptic cell is initially setup to be parallel to the longer axis of the ellipse (i.e., the initial distribution of the protrusion signal is a gradient from high in the left to low in the right). Over time, the interface rotates and eventually aligns with the shorter axis of the ellipse. To see how various model parameters, influence the steady-state protrusion and retraction distributions in the reaction-diffusion submodel, a rectangular (with an aspect ratio of 1:3) cell shape is used to simulate approximately a quasi-1D domain. The simulation results for parameter ζ_a , ζ_0 , K_0^ξ , and K_{off}^ξ are plotted in Fig. 3C-F. One can see that change of these parameters can all shift the position of the interface and the peak value of ξ at the steady state.

Focal adhesion stress-dependent protrusion signal distribution

The reaction-diffusion submodel described above can account for the polarization of the protrusion signal, but it cannot explain the phenomenon observed in the previous study [15] in which the membrane protrusion localized to the four corners of the square cell. As shown in Fig. 4A, the reaction-diffusion submodel alone predicts a polarized pattern for the protrusion signal distribution in a square cell.

Our previous studies showed that localization of the traction stress (which is equal to the focal adhesion stress) at the corners of the square cell is simply due to the mechanics principle of static equilibrium of an elastic body [19]. Based on that, we argue that protrusion signal and focal adhesion assembly can be enhanced by the mechanical stress in the focal adhesion. This hypothesis is implemented in our model by introducing the K_T^ξ term in Eq. (6) and the K_T^ρ term in Eq. (16).

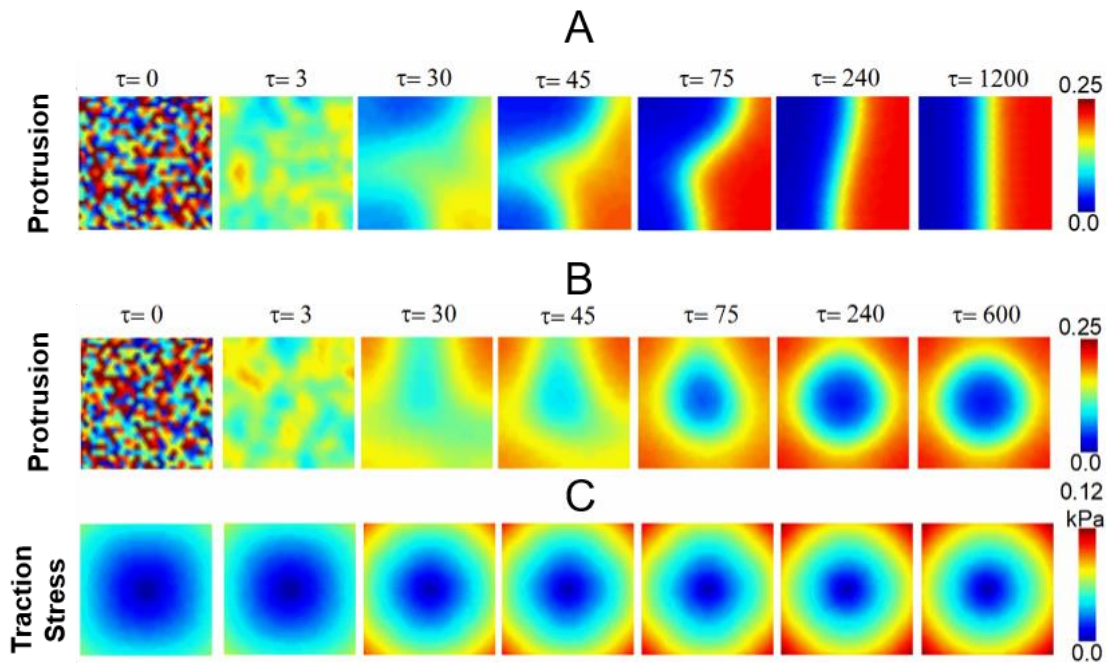


Figure 4. The effect of mechanobiochemical coupling to the protrusion signal.

(A) Protrusion signal ξ forms gradient pattern spontaneously with random initial perturbation. (B) Traction stress contour, with coupling protrusion signal. (C) Protrusion signal ξ forms circular pattern, with coupling traction stress, (i.e., turning on stress dependent activation parameter, $K_T^\xi = 0.45$)

We define the system of equations consisting of Eq. (1)-(9) and Eq. (16)-(19), where K_M^ξ and K_M^ρ are set to be zero, as the contraction-reaction-diffusion submodel. Simulations results of the contraction-reaction-diffusion submodel for the square shape are presented in Fig. 4B-C, showing the localization of high traction stress (Fig. 4B), and protrusion signal (Fig. 4C) at the corners of the square cell. In a dynamic process, the localization to the corners is due a positive feedback loop in the contraction-reaction-diffusion submodel: larger traction stress T leads to bigger ρ (Eq. (16)), larger ρ leads to bigger k_{cs} (Eq. (18) and (19)), bigger k_{cs} results in larger traction stress T (Eq. (4)).

The role of the cytoskeleton asymmetry to the persistent migration

In this model, we introduce a cytoskeleton-asymmetry function $f_M(s)$ to be able to explicitly control the directional persistence of migration. Figure 5 illustrates the role of function $f_M(s)$ in cell migration, in which the first two rows correspond to the simulation results of the protrusion signal and traction stress when the cytoskeleton

asymmetry is turned off (i.e., setting $K_M^\xi = K_M^\rho = 0$), while the bottom two rows correspond to the simulation when the cytoskeleton asymmetry is on. Both simulations start with a circular cell and polarized protrusion signal (i.e., we initialize a spatial gradient for the distribution of the protrusion signal within the cell domain). When the cytoskeleton asymmetry is turned off (see the top two rows), the cell first becomes an elliptic shape due to the protrusion on the front of the cell and the retraction on the back of the cell. The interface line that divides the high and low protrusion signal regions is parallel to the longer axis of the ellipse. Then the cell front turns due to the turning of the interface line towards the shorter axis of the ellipse. On contrary, when the cytoskeleton asymmetry is turned on (bottom two rows), the cell shape becomes elongated in the dynamic equilibrium of the process of protrusion and retraction, and the cell preserves migration direction.

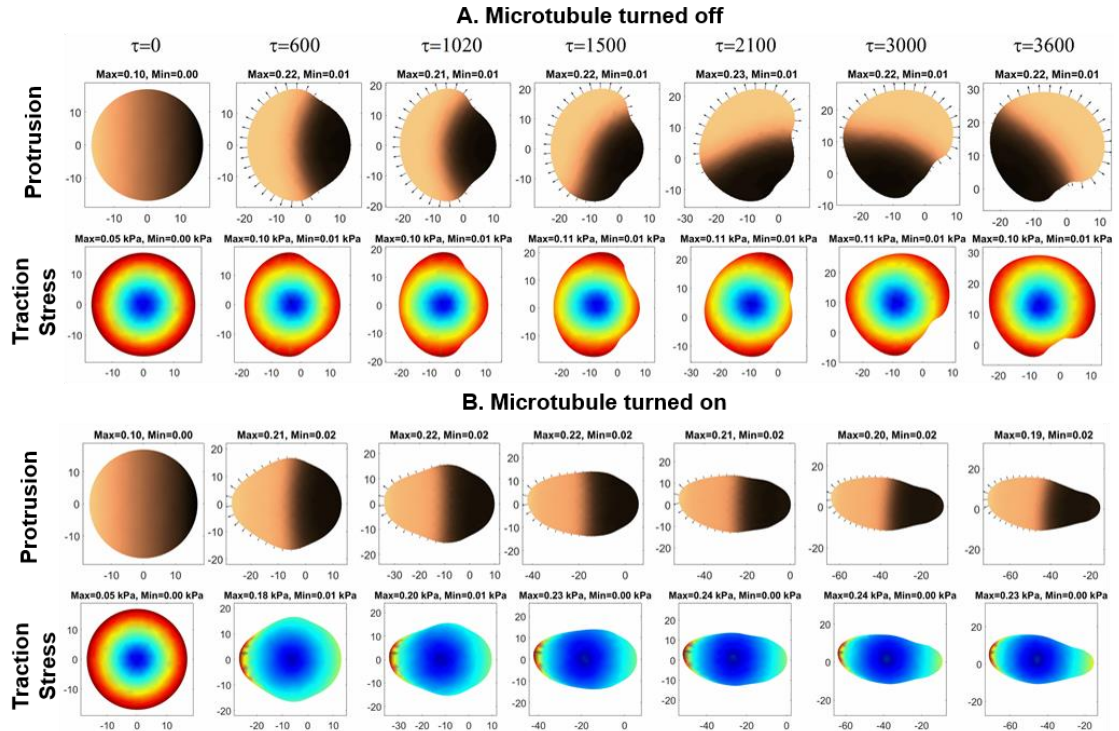


Figure 5. The role of the cytoskeleton asymmetry to the persistent migration. The first and third rows: protrusion signal. The second and fourth rows: traction stress. For the first 2 row the Microtubule effect is simply turned off by setting the $K_M^\rho = 0$ and $K_M^\xi = 0$ For the third and fourth row, we just simply turned on the microtubule by setting $K_M^\rho = 0.1$ and $K_M^\xi = 0.05$.

Comparison with experimental data

To validate the cell migration model and to help estimate the modal parameters, live-cell imaging and traction-force microscopy experiments were conducted with MDA-MB-231 breast cancer cells. The quantitative experimental data for the cell shape and traction stress distribution during the cell migration process were obtained (Fig. 6, rows 1 and 3). The traction forces obtained in the micro-post experiment has been converted to traction stress by dividing the force on each post by an area a_p , where a_p is the surface area per post. The cell shape at each time snapshots were extracted and used in the model simulations as the input. In the simulations, the protrusion/retraction movement of the cell was turned off. The model parameters associated with the mechanical properties of the cytoskeleton and cell-substrate adhesion were manually tuned such that both the pattern and magnitude of the predicted traction stress distribution best match the experimental results (see Fig. 6). As a result, we found that one set of model parameters can be found to yield good matching for the most of the time frames in the whole course of migration period presented in Fig. 6.

Note that in one of the experimental image (indicated by the arrow head), the high traction stress was not located at the margin of the cell, which is different than the corresponding model calculation. this discrepancy is interpreted as follows. The modeling results were from the steady state of the dynamic simulations, under the assumption that the time scale of cell shape change is much slower than other time scales in the dynamic model. The model also lacks the consideration of spatial and temporal heterogeneities in the cell. As a result, our present mathematical model will always predict higher traction stress at the edge of the cell because of the principle of static equilibrium. In the experiment, the upper-right region of the cell at $t = 165$ mins is the tail that was retracting. The tail may not retract in a normal speed, leaving a tail with weak adhesion and thus small traction stress.

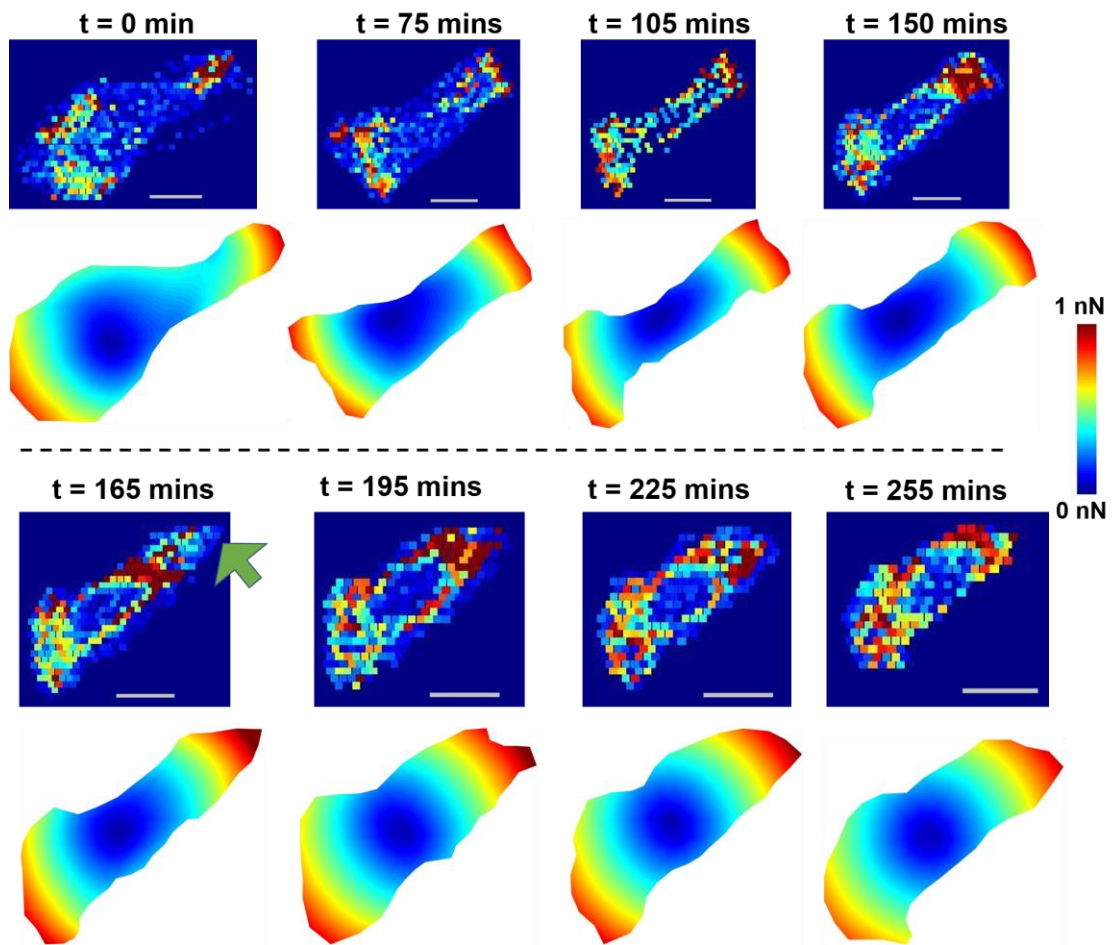


Figure 6. Experimental results using micropillar test. The scale bars in the experimental figures are 10 μm . The upper limit for the color bar for both experimental and simulation figures are 1 nN.

For the experiments in Fig. 6 center to center distance for microposts are 2 μm , center to center is the distance from all the adjacent microposts (i.e., one side of the hexagon shape). The boundaries are determined manually based on phase images. The post has 4.77 μm height, 0.8 μm diameter, and thus spring constant = 1.389 nN/ μm ,

and effective modulus is 2.44 kPa. Images intervals are 15 mins. migration of MDA-MB-231 breast cancer cells.

Simulation of durotaxis

Durotaxis is a term coined by Lo et al. [10], which refers to the substrate rigidity-guided cell migration. They showed in the *in vitro* experiment where a fibroblast cell crawls from the stiffer side of the substrate toward the softer side, the cell made a 90-degree turn at the interface to avoid migrating into the softer region. A conceptual two-step theory consisting of the force generation and mechanotransduction has been proposed previously by Lo et al. to explain the durotaxis. A simple mechanics model has been presented by us previously to explain how exactly the larger focal adhesion stress is generated at the stiffer region of the substrate [14]. We showed that static equilibrium of the adherent cell along can yield the disparate traction stress on regions of different rigidity. In this study, we integrate the elasticity model with the reaction-diffusion equations to form a contraction-reaction-diffusion system.

Here the dynamic model of single-cell migration is used to reproduce durotaxis phenomenon *in silico*. Cells started as a polarized circular shape and placed on the stiffer region of the substrate. The cell then crawls toward the softer region (i.e., left side). The results from two simulations are presented in Fig. 7. The only difference between these two simulations is the stress-dependent protrusion signal parameter K_T^ξ : relatively high for the simulation I (top three rows) and low for the simulation II (bottom three rows). Note that parameter K_T^ξ regulates the level of force-dependent activation of protrusion signal. At relatively low value of K_T^ξ (top three rows), the cell

crosses the interface with a slight change of cell shape. At high value of K_T^ξ , the cell makes a turn at the stiff-to-soft interface and then crawls along the interface. The turning of the cell at the interface is caused by the positive feedback loop mentioned previously in Fig. 4: larger substrate stiffness leads to larger traction stress, larger traction stress leads to higher level of focal adhesion and protrusion signal, which results in change of migrating direction at the interface. These simulation results show that our model can successfully simulate durotaxis phenomenon.

Our simulations demonstrate that the cell can sense the non-specific mechanical cues of its microenvironment through a mechanobiochemical system (see Fig. 2). The key and the starting part of this system is the active contraction of the cell. Without the actomyosin contraction, no forces will be generated and the mechanosensors will not be activated.

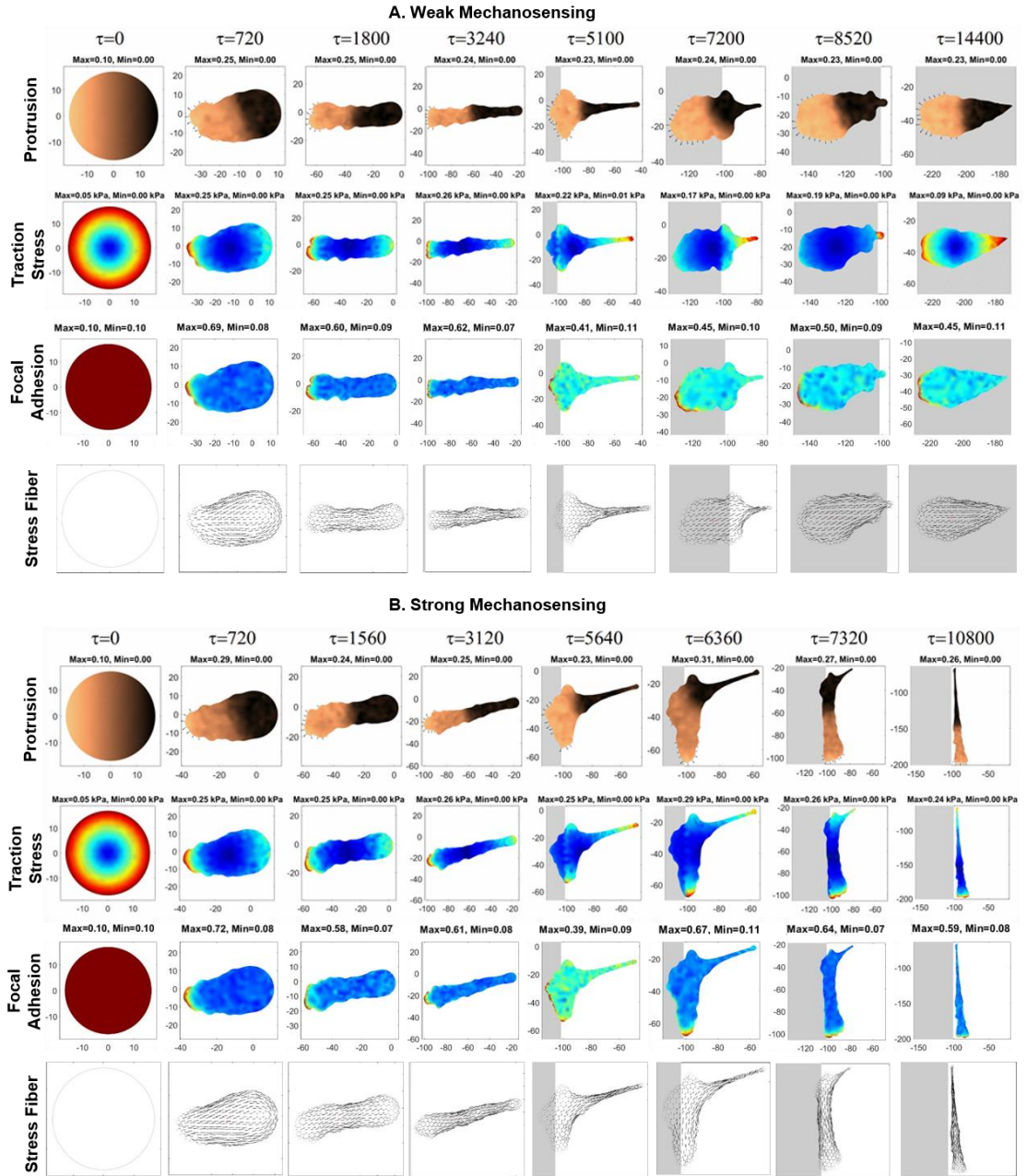


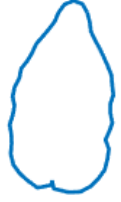
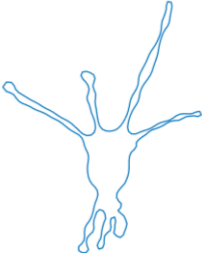
Figure 7. Simulation of durotaxis. The first and third rows: protrusion signal. The second and fourth rows: traction stress. Top two rows: higher stress dependent parameter, $K_T^\xi=0.6$, durotaxis happens. Bottom two rows: lower stress dependent, $K_T^\xi=0.4$, cell passes the interfaces.

Cell shape

Cell shape is an emergent property of a cell during cell spreading and migration. Here we demonstrate how the cell shape can be changed by varying the model parameters. The parameter space of the model was searched to identify the cells of different shapes. To quantitatively characterize the cell shape, we define two dimensionless numbers: the roundness and branchness numbers. The roundness number, denoted by R_n , was defined as $R_n = A/(\pi\tilde{r}^2)$ where A is the area of the cell, \tilde{r} is the radius of the circle that circumscribe the cell boundary [3]. The roundness number R_n takes maximal value of 1 when the cell shape is a perfect circle and is smaller than 1 for any other shapes. It is useful in distinguish between elongated and rounded shapes, but may fail to distinguish between the elongated and dendritic shapes. The branchness number B_n is defined as $B_n = L/(2\pi\tilde{r})$, where L is the perimeter of the cell. The branchness number B_n has a lower bound of $2/\pi \approx 0.64$ when the cell shape approaches a strip with zero width, and becomes large when the cell shape is dendritic.

Both the brute-force search and genetic algorithm were used for the parametric study. As shown in Table 1, three characteristic shapes were identified in the parameter space search: elongated, rounded, and dendritic shapes, with their roundness and branchness numbers listed. The values of some key model parameters that corresponds to these three characteristic shapes are also listed in the table. Note that the parameter values are given as ranges, indicating the regions of the parameter space where these characteristic shapes emerge.

Table 1. Characteristic cell shape simulated by the cell model

Cell Shape Parameters	 Roundness = 0.47 Branchness = 0.78	 Roundness = 0.76 Branchness = 0.93	 Roundness = 0.1 Branchness = 1.43
$\xi_p (1 \mu m^{-2})$	0.06 - 0.15	0 - 0.01	0.13 - 0.38
c_p	0.11 - 0.27	0.6 - 0.77	0.56 - 0.93
c_r	0.03 - 0.08	0.03 - 0.04	0.01 - 0.14
K_M^ξ	0.06 - 0.15	0.28 - 0.41	0.01 - 0.66
K_T^ξ	0.06 - 0.15	0.22 - 0.31	0.36 - 1.44
$\rho_a (1 \mu m^{-2})$	0.39 - 0.51	0.24 - 0.35	0.29 - 1
K_M^ρ	0.07 - 0.15	0.01 - 0.02	0.01 - 0.44

One of the most common observation from analyzing the simulation results was that the total focal adhesion is an important parameter and plays crucial role in cell morphology. Altering the focal adhesion, changes the cell shape drastically.

Conclusions

In this work, we developed a computational model that integrates the biomechanics and biochemistry of the cell spatiotemporally at the whole-cell scale. Biomechanical and biochemical events and processes were treated as modules, between which cross-talks are defined. We have shown that the reaction-diffusion submodel can simulate cell polarization (head-to-tail formation), the contraction-reaction-diffusion submodel can simulate the localization of protrusion signal to the corners of the square cell, and the cytoskeleton-asymmetry module can simulate the persistent migration. Importantly, by coupling the mechanosensing with membrane protrusion signals, we demonstrated that this mechanobiochemical model can simulate substrate rigidity-guided cell migration (i.e., durotaxis). Finally, the full model, when applied to dynamics of cell migration, can predict cell shape formation, i.e., cellular morphogenesis.

Our computational model incorporates the reaction-diffusion equations with continuum mechanics equations, thus enabling *in silico* studies of the coupling between the biochemistry and mechanobiology. The computational model and the computer program developed here can be used to test hypothesis and gain understandings of the complex system of living cells and tissues. The finite element method-based numerical implementation of the model makes the computational model accurate and efficient in simulating cells with irregular shapes. The modular approach of the development of this phenomenological model makes it easy to be extended to incorporate more biophysical principles. The extension of this single-cell migration

model to microtissues or monolayers will be discussed in detail in a forthcoming paper.

Acknowledgments

H.Y. acknowledge funding support from the ASME Haythornthwaite Research Initiation Grant Award.

References

- [1] G. Danuser, J. Allard, and A. Mogilner, “Mathematical modeling of eukaryotic cell migration: insights beyond experiments,” *Annu Rev Cell Dev Biol*, vol. 29, pp. 501–528, 2013.
- [2] P. Devreotes and A. R. Horwitz, “Signaling networks that regulate cell migration,” *Cold Spring Harb Perspect Biol*, vol. 7, no. 8, p. a005959, 2015.
- [3] J. Satulovsky, R. Lui, and Y. Wang, “Exploring the Control Circuit of Cell Migration by Mathematical Modeling,” *Biophys. J.*, vol. 94, no. 9, pp. 3671–3683, 2008.
- [4] A. J. Ridley *et al.*, “Cell migration: integrating signals from front to back,” *Science*, vol. 302, no. 5651, pp. 1704–9, Dec. 2003.
- [5] M. D. Onsum and C. V Rao, “Calling heads from tails : the role of mathematical modeling in understanding cell polarization,” pp. 74–81, 2009.
- [6] R. Wedlich-Soldner, S. Altschuler, L. Wu, and R. Li, “Spontaneous cell polarization through actomyosin-based delivery of the Cdc42 GTPase,” *Science (80-.)*, vol. 299, no. 5610, pp. 1231–1235, 2003.
- [7] A. F. M. Marée, A. Jilkine, A. Dawes, V. A. Grieneisen, and L.

Edelstein-Keshet, “Polarization and movement of keratocytes: a multiscale modelling approach,” *Bull Math Biol*, vol. 68, no. 5, pp. 1169–1211, Jul. 2006.

[8] P. a. Iglesias and P. N. Devreotes, “Biased excitable networks: How cells direct motion in response to gradients,” *Curr. Opin. Cell Biol.*, vol. 24, no. 2, pp. 245–253, 2012.

[9] Y. Xiong, C.-H. Huang, P. A. Iglesias, and P. N. Devreotes, “Cells navigate with a local-excitation, global-inhibition-biased excitable network,” *Proc. Natl. Acad. Sci.*, vol. 107, no. 40, pp. 17079–17086, 2010.

[10] C. M. Lo, H. B. Wang, M. Dembo, and Y.-L. Wang, “Cell movement is guided by the rigidity of the substrate,” *Biophys. J.*, vol. 79, pp. 144–152, 2000.

[11] M. P. Sheetz and J. Dai, “Modulation of membrane dynamics and cell motility by membrane tension,” *Trends Cell Biol.*, vol. 6, no. 3, pp. 85–89, 1996.

[12] M. P. Sheetz, D. P. Felsenfeld, and C. G. Galbraith, “Cell migration : regulation of force on extracellular-matrix-integrin complexes,” *Trends Cell Biol.*, vol. 8, no. 97, pp. 51–54, 1998.

[13] A. del Rio, R. Perez-jimenez, R. Liu, P. Roca-Cusachs, J. M. Fernandez, and M. P. Sheetz, “Stretching Single Talin Rod Molecules Activates Vinculin Binding,” *Science (80-.)*, vol. 323, no. 5914, pp. 638–641, Jan. 2009.

[14] B. Marzban, X. Yi, and H. Yuan, “A minimal mechanics model for mechanosensing of substrate rigidity gradient in durotaxis,” *Biomech. Model. Mechanobiol.*, vol. 1, pp. 1–8, 2018.

[15] K. K. Parker *et al.*, “Directional control of lamellipodia extension by constraining cell shape and orienting cell tractional forces,” *Faseb J*, vol. 16, no. 10,

pp. 1195–1204, 2002.

[16] A. Rahman *et al.*, “Vinculin regulates directionality and cell polarity in two- and three-dimensional matrix and three-dimensional microtrack migration,” *Mol. Biol. Cell*, vol. 27, no. 9, pp. 1431–1441, 2016.

[17] M. Yao *et al.*, “Force-dependent conformational switch of α -catenin controls vinculin binding,” *Nat. Commun.*, vol. 5, Jul. 2014.

[18] F. Twiss and J. De Rooij, “Cadherin mechanotransduction in tissue remodeling,” *Cell. Mol. Life Sci.*, vol. 70, no. 21, pp. 4101–4116, 2013.

[19] H. Yuan, B. Marzban, and K. K. Parker, “Myofibrils in Cardiomyocytes Tend to Assemble Along the Maximal Principle Stress Directions,” *J. Biomech. Eng.*, 2017.

[20] H. Yuan, B. Marzban, and K. K. Parker, “Myofibrils in Cardiomyocytes Tend to Assemble Along the Maximal Principle Stress Directions,” *J. Biomech. Eng.*, vol. 139, no. 12, 2017.

[21] B. Marzban, X. Yi, and H. Yuan, “A minimal mechanics model for mechanosensing of substrate rigidity gradient in durotaxis,” *Biomech. Model. Mechanobiol.*, vol. 17, no. 3, pp. 915–922, Jun. 2018.

[22] G. Forgacs and S. A. Newman, *Biological Physics of the Developing Embryo*. Cambridge: Cambridge University Press, 2005.

[23] A. F. M. Maree, V. A. Grieneisen, and L. Edelstein-Keshet, “How cells integrate complex stimuli: The effect of feedback from phosphoinositides and cell shape on cell polarization and motility,” *PLoS Comput. Biol.*, vol. 8, no. 3, 2012.

[24] H. V. Prentice-Mott *et al.*, “Directional memory arises from long-lived

cytoskeletal asymmetries in polarized chemotactic cells,” *Proc. Natl. Acad. Sci.*, vol. 113, no. 5, p. 201513289, 2016.

[25] S. J. Altschuler, S. B. Angenent, Y. Wang, and L. F. Wu, “On the spontaneous emergence of cell polarity,” *Nature*, vol. 454, no. 7206, pp. 886–889, 2008.

CHAPTER 4 :

RDC-CELL: A computational model and package for whole-cell multiphysics simulations of cell monolayer

by

Bahador Marzban, Hongyan Yuan*

To be submitted in PLOS ONE Computational biology

*Corresponding author:

Hongyan Yuan

Department of Mechanical, Industrial and Systems Engineering,

University of Rhode Island,

331A Pastore Hall, 51 Lower College Road, Kingston, RI 02881, USA

USA phone: +1-401-874- 2774

Email: hongyan_yuan@uri.edu

Abstract

Cell morphogenesis is a fundamental process involved in tissue formation. One of the challenges in the fabrication of living tissues *in vitro* is to recapitulate the complex morphologies of individual cells. Despite tremendous progress in understanding biophysical principles underlying tissue/organ morphogenesis at the organ level, little work has been done to understand morphogenesis at the cellular and microtissue level. In this work, we extend the previously developed 2D computational model for studying cell morphogenesis in monolayer tissues. We have added the cell-cell interaction module and nucleus module to the model. The model integrates the biochemical and mechanical activities within individual cells spatiotemporally. The computer program can simulate tens to hundreds of cells interacting with each other and with the elastic substrate on desktop workstations efficiently. The simulations demonstrated that our computational model can be used to study morphogenesis in cell monolayers.

Keywords: Cell monolayer, Cell motility, Collective cell migration, Virtual-Cell simulation, reaction-diffusion

Introduction

Tissue/organ morphogenesis is a complex process occurring at multiple scales. Focusing on the whole organ scale, considerable research has been devoted to elucidation of the physical principles underlying the formation of the overall morphologies of organs [1]–[3], as well as the nutrient consumption and transport in

bioreactors [4] for tissue engineering. In these whole-organ level studies, information at the individual cell level has been homogenized or ignored. At the other extreme of the length scale, the genetic and molecular causes that dictate the tissue/organ formation have been intensively studied [5]. There is gap between our understanding of how phenotypic morphologies at the organ level emerge from genetic information. Studies at the cellular and microtissue level play an indispensable role to bridge these two scales.

The phenotypic morphologies of cells including cell shape and cytoskeleton architecture, cell-ECM and cell-cell adhesions, can be best seen by comparing four types of tissues: muscle tissue, nerve tissue, epithelial tissue, and connective tissue. Each of these different tissues exhibit characteristic morphologies in cell shape and cytoskeleton architecture. These four basic types of tissues are arranged spatially in various patterns (e.g., sheets, tubes, layers, bundles) to form organs. Gene expression only dictates what proteins to make and subsequently what biochemical reactions to carry out, the emergence of spatial morphologies must be determined by biomechanical principles and the coupling between biomechanics and biochemistry [6]–[8]. Mechanobiochemical coupling is exemplified by the recent discoveries in the field of mechanobiology. Cellular functions including cell migration and cytoskeletal dynamics that are closely related to cell morphogenesis, have been shown to be regulated by various mechanical cues such as matrix elasticity [9], matrix topology [10]–[15], matrix dimensionality [16]–[20], cell-ECM/cell-cell adhesions [21], and cell shape constraints [22]–[25]. Therefore, mechanical and geometric properties of

cells and their microenvironments at the length scale comparable to single cells can have a dominant effect on the microscopic tissue morphology.

Mathematical models based on reaction-diffusion equations at the cellular scale were developed to understand spatial pattern formation in the context of cell migration, such as cell polarization [26], [27] and cell morphogenesis [28], [29]. However, biochemical models lack the consideration of mechanotransduction thus cannot adequately capture cell morphogenesis. Biomechanics models were developed to interpret specific aspects of cell spreading, for example, the distribution patterns of traction force [30], cell adhesion [31], and cytoskeleton dynamics [32]–[36]. In contrast, biomechanics models lack consideration of biochemical signaling and thus fail to account for biochemical regulations. A thorough understanding of cell and microtissue morphogenesis will require the elucidation of how the mechanical and biochemical events are spatiotemporally integrated at the cellular scale.

In this work. We extended the single-cell model (See Chapter 3) to multicellular monolayer model by adding a module of the cell-cell interaction. Finite element method is used to solve the resulting system of partial differential equations and the model was implemented in an in-house MATLAB code.

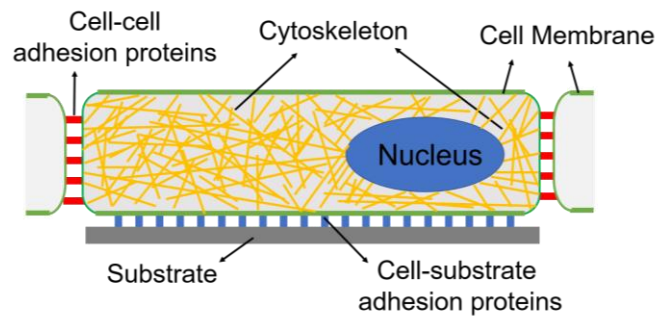
Model Description

Physical and mathematical domains

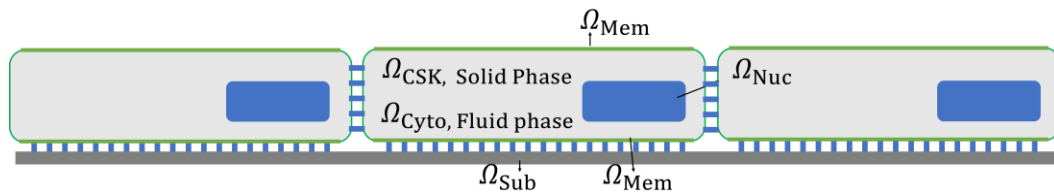
Four physical domains are defined for the cell: solid phase cytoskeleton domain Ω_{CSK} , fluid phase cytosol domain Ω_{Cyto} , membrane domain Ω_{Mem} , and nucleus domain Ω_{Nuc} (See figure 1A). The elastic substrate (underneath the cell) domain is denoted by

Ω_{Sub} . In the cell membrane domain Ω_{Mem} and cytosol domain Ω_{Cyto} , reaction-diffusion equations of diffusive molecules are formulated to model the protrusion and retraction signals. In the cytoskeleton domain Ω_{CSK} , solid mechanics equations are formulated, and the mechanical stresses experienced by the cell are solved. The present computational model is concerned with the cell monolayer adhering to a flat substrate. Each cell is modeled as a two-dimensional (2D) continuum, which reflects the flatness of the lamellipodia for cells cultured on 2D flat substrates. Because 2D model of the cell is adopted, the physical domains Ω_{CSK} , Ω_{Cyto} , Ω_{Mem} , and Ω_{Sub} can be described by the same mathematical domain, denoted by Ω .

A



B



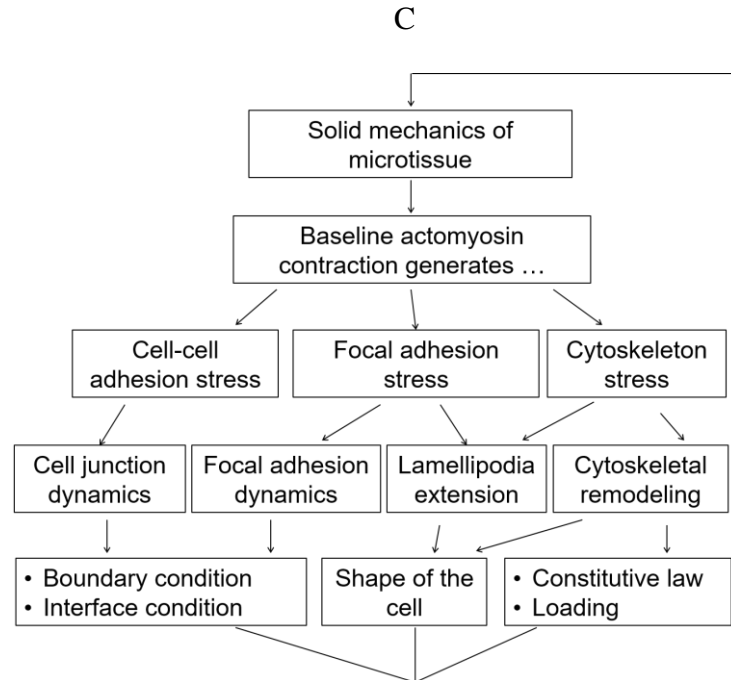


Figure 1. Schematic illustrations of the cell model. (A) Schematic of cytoskeleton of the cell and main components of the cell’s structure. (B) Schematic illustrations of the physical domains in the cell model and cell–cell interaction. (C) The mechanobiochemical coupling and feedback loops in the cell morphogenesis model.

Nucleus deformation and movement

The nucleus is modelled as an elastic structure that deforms upon the compression of the cell membrane and moves with the cytoskeleton. In the present model, there are no mechanotransduction associated with the nucleus. Rather, the nucleus is a passive material and can resist deformation and contribute to the shape of the cell in cases cell are elongated or compressed. In the finite element-based numerical implementation, the nucleus is discretized into networks of nonlinear springs connected at the nodes. The configuration of the network is updated using Newton’s equation of motion of the nodes. The numerical implementation concerning the passive nucleus model will be

presented in a later publication where the numerical algorithm and software package is described in detail.

Cell-cell interaction module

In cell monolayers where cells are connected mechanically by cell-cell adhesion, the static equilibrium of the cells depends on the cell-cell contact [37]–[40] in addition to cell-substrate adhesions. To simulate the dynamic process of formation and dissociation of cell-cell adhesion, a stochastic model is used to determine the binary state of the cell-cell adhesion as follows. When cell-A and cell-B is in close contact, the state of the cell-cell adhesion can be either “on” or “off”. The “on” state indicates that the cell-cell adhesion is established. The “off” state indicates that although two cells are in close contact, they do not adhere to each other. The probability of the “off” state per unit edge length and unit time is denoted by cell-cell break rate parameter φ . when the cell-cell adhesion state is “on”, the stress between cell-A and cell-B, P_i , is calculated as

$$P_i = k_{cc}(u_i^A - u_i^B) \quad (1)$$

where u_i^A and u_i^B are the displacement of cell-A and cell-B at their edges (where the cell-cell adhesion is formed), respectively, and k_{cc} is the spring constant of the cell-cell linkage.

Mechanobiochemical coupling

These different modules are coupled through the mechanics of the tissue. As illustrated in Figure. 1B, through molecular scale mechanotransduction pathways,

mechanical stresses in the cell are converted into biochemical activities, which in turn regulate the assembly/disassembly of macromolecular of the cell. The macromolecular assembly and disassembly alter the structural, geometrical, and material properties of the cell, which, according to the continuum/structural mechanics theory, will subsequently change both the internal stress (cytoskeleton stress) and stress at the boundary (cell-matrix and cell-cell adhesion stress). Thus, mechanics of the cell, biochemical activities, and macromolecular assemblies are coupled through mechanobiochemical feedback loops as depicted by the arrows in Figure. 1B.

Numerical Implementation

The cell monolayer model has been implemented in an in-house code. Finite element method has been used to solve partial differential equations resulted from reaction-diffusion and elasticity equations. Explicit Euler scheme has been used for the time integration. Due to extremely large deformation experienced by the cells during the cell migration, Lagrangian mesh has been adopted and 3-node triangle element has been used.

In terms of the algorithm implementation, we have 4 major part; *data input, main function, cell migration, remeshing*. Figure 3 shows a detailed algorithm that being used for the proposed model. The flowchart shows the main flow of the algorithm on the left side and on the right side it shows the main tasks within every loop. The flowchart introduces the core operations and almost each core operation itself consists of several subroutines (there is a list of major subroutines in the Appendix A). We

also use a *flags-based* coding, meaning different modules of the code can be either turned on /off or switched based on the scenarios. An example for the former is turning the cell migration on or off and an example for the latter is switching between initial distribution of the signals from random to constant or gradient pattern.

First, a data structure name *para* is used for the parameters input (see table 1 in appendix B for the parameters used in this study), the data structure will be initialized for feeding into the main function. Note that for simulating different scenarios (e.g., static cell, moving cell, cell pair, multi cell, etc.) different drivers are being used for variables initialization. While the main computational core of the algorithm is the same for all scenarios, different postprocessing algorithms associate with each scenario has been utilized to extract and visualize the results. Driver calls the main function and time integration begins in the main function. Within the time integration loop, the first procedure at every time step is storing the data from current workspace and if the *flag.plot_result* is on, results will be plotted during the simulation. Next step is updating the microtubule vector since it will be used for updating the signals concentrations (i.e., protrusion, retraction, focal adhesion), after that we solve and update for the reaction-diffusion equations (protrusion and retraction signals) and a rate equation for updating the focal adhesion. Also, we will update the Substrate boundary condition and apply adhesive island for different scenarios (i.e., assigning zero focal adhesion to the different zones of the substrate that we do not want the cells to attach). Here, if the *flag. Update_mechanics* is on, solver elasticity solves for displacement resulted from contraction. Next, we will update the stress fiber.

Second, algorithm decides whether enters into the *migration* or not. At this level, For a moving cell simulation, if the *flag.cell_migration* is on and the time is bigger than equilibrium time, the algorithm enters the *migration* and cell starts to move. The equilibrium time is necessary since the signals distribution initially are random and it must reach to a steady state and cell polarization, this in turn will facilitate the cells to move around. Now, within the *migration* loop, the first stage is updating the nucleus. Second procedure is updating the nodal coordinates by updating the growth and retraction displacement of the nodes. Note that in the simulations of the movement of the cell, the nodal spatial coordinates are updated based on protrusion equation and retraction equation. Consequently, updating other variables such as element area, and cell area, etc. is the next task.

Third, algorithm decides about the *remeshing*. There are two different criteria to check whether the resulted deformation from the growth and retraction causing significant distortion to the triangular elements or not. Therefore, if the criteria for remeshing satisfies, automatic mesh generation algorithm runs and creates high quality and optimized triangular meshes for the deformed cell. At the end of the *remeshing*, since the elements and nodal coordinates for the elements has been changed after the remeshing, algorithm needs to update all the variables previously defined on the old elements and nodes to the new set of elements and nodes. This updating is being performed using the scattered interpolation functions. Therefore, mesh transfer for the field variables will be performed between the old and new mesh. Second task after *remeshing* is updating the Mass (M) matrix and the stiffness (K) matrix since the connectivity matrix for the elements has been changed due to remeshing. Here,

avoiding the remeshing and calculation of the mass (M) and stiffness matrix (K) was considered to increase the execution speed of the algorithm. At this point we also update the list for the nucleus and cell edge contact. We also update the cell-cell contact (i.e., updates the cell neighbors list) and adhesion list using a Monte Carlo based model.

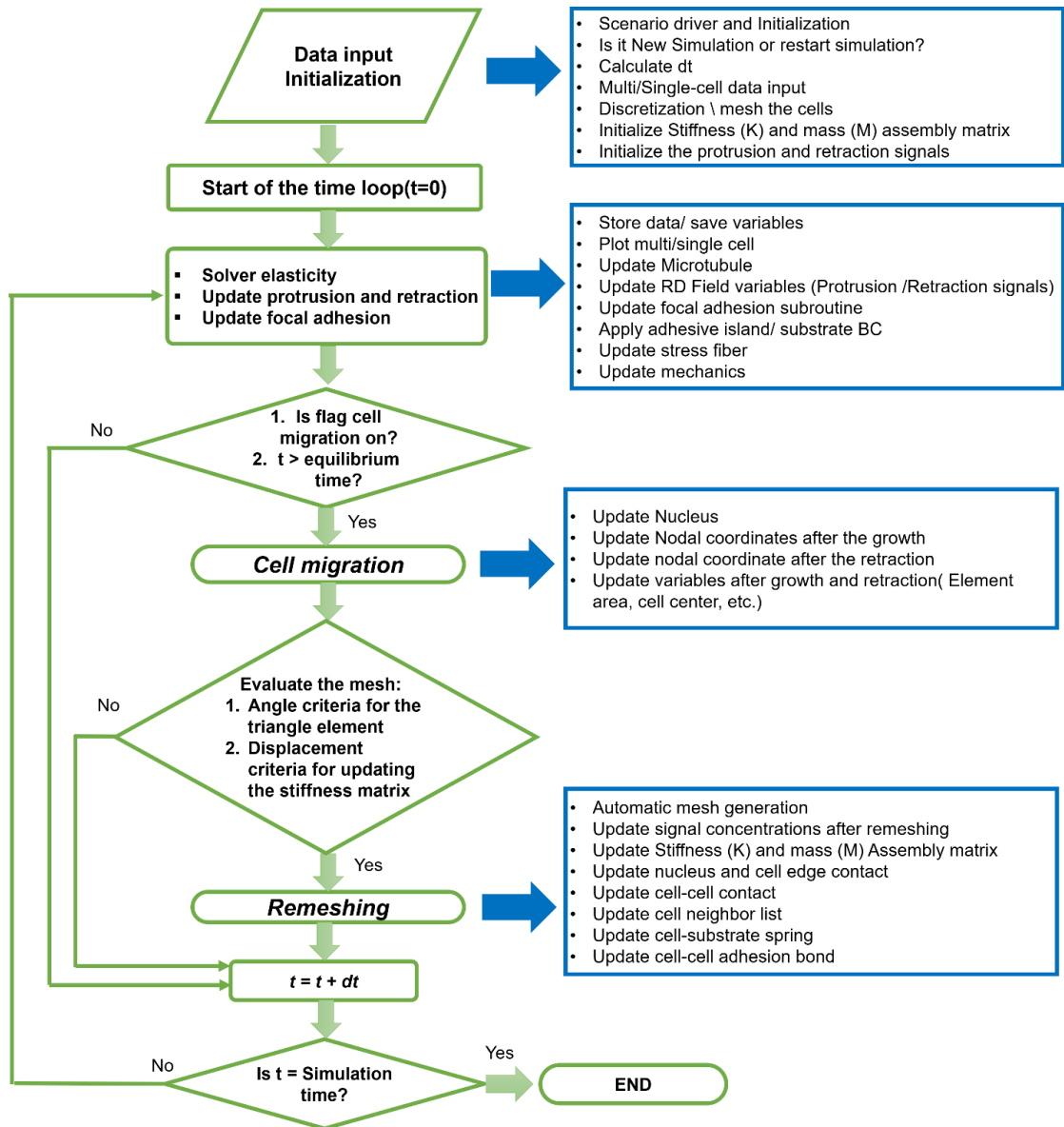


Figure 2. Detailed flow chart of the cell monolayer algorithm.

Case study: Collective cell migration in monolayer tissue

Collective cell migration has been studied *in vitro* where a confluent monolayer of cells crawls on a flat 2d substrate [41], [42]. Here we conduct the *in-silico* modeling of cells crawling in monolayers, as shown in Fig. 3. Total of 26 cells are confined in an adhesive region of a circular shape with a hole in the middle. The inner and outer radius of the adhesive region are 30 μm and 83 μm , respectively. To study the role of intercellular adhesion in collective cell migration, we performed two simulations: case-I (cell-cell adhesion is turned off) and case-II (cell-cell adhesion is on). The dynamic simulations start with circular cells seeded onto the adhesion region. Overtime, cells polarize, spread, and migrate.

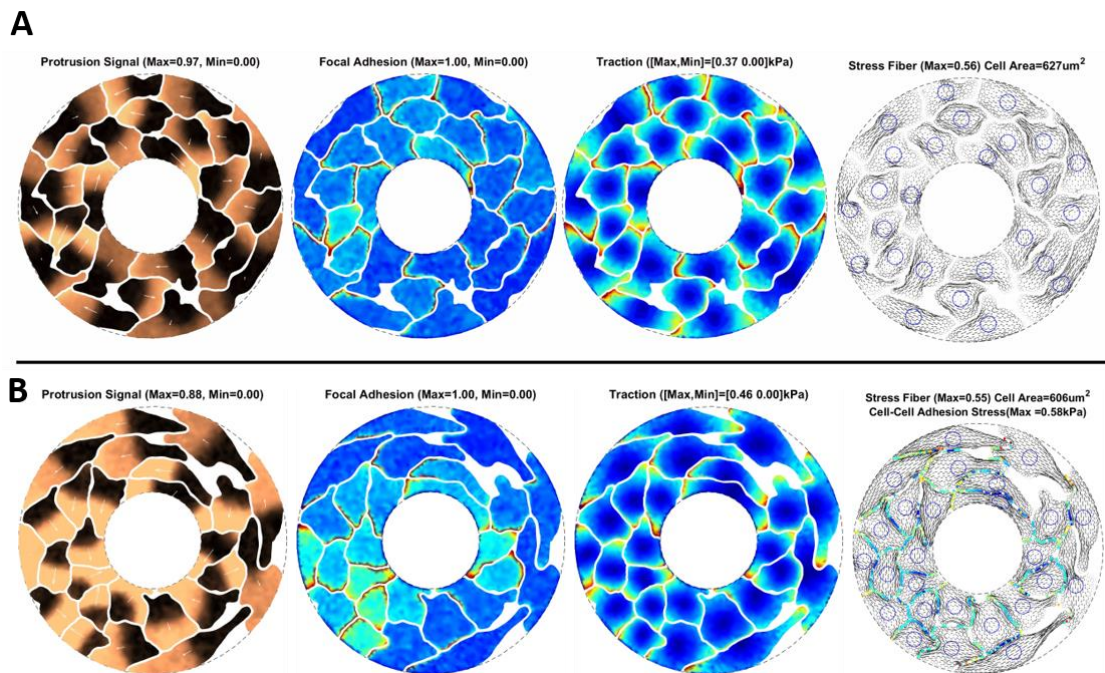


Figure 3. Collective cell migration in confluent monolayers. (A) Simulation snapshots of cells in confluent monolayers without cell-cell adhesion, (B) Simulation snapshots of cells in confluent monolayers with cell-cell adhesion. Four subfigures in each row show protrusion signal, focal adhesion, traction stress, and stress fiber, respectively. In the stress fiber figures, fourth column, circles on the cells are the nucleus. Parameter value used: $k_{cc} = 1 \text{ kPa}$.

Figure 3A and 3B show the simulation snapshots of cells in the confluent monolayers for case-I and case-II, respectively, where the migration direction of each cell can be seen in the protrusion subfigures. The cell-cell adhesion stress is zero for case-I (Fig. 3A) since it is turned off. In case-II, because of the presence of the cell-cell adhesion, cell contraction is balanced by the cell-cell adhesion, rather than purely by the cell-substrate adhesion.

Conclusions

In this work, we developed a 2D computational model for studying cell morphogenesis in monolayer tissues. Because of the complex nature of the living cell, the model, despite being phenomenological, is still sophisticated. Conceptually, we divide the full model into modules, and studied the behaviors of the submodels, as well as the couplings between modules. We have showed that the reaction-diffusion submodel can simulate cell polarization (head-to-tail formation), the contraction-reaction-diffusion submodel can simulate the localization of protrusion signal to the corners of the square cell, and the cytoskeleton-asymmetry module can simulate the

persistent migration. We also demonstrated that this mechanobiochemical model can simulate durotaxis and cell morphogenesis in monolayers.

Our computational model incorporates the reaction-diffusion equations with continuum mechanics equations, thus enabling *in silico* studies of the coupling between the biochemistry and mechanobiology. The finite element method-based numerical implementation of the model makes the computational model efficient in simulating cell monolayers with tens to hundreds of cells on desktop workstations [43][44], [45]. In the future, The model can be further developed and extended to a 3Dimensional model meshless methods such as material point methods or peridynamics model can be also used to deal with the remeshing in 3D [46], [47]. The computational model and the computer program can be used to test hypothesis and gain understandings of the complex system of living cells and tissues. The model can be further developed to study the effect of various external cues such as modulated and tailored acoustic wave on biological cells, which has been recently reported to be used as a cancer cell separation technique [48][49] .

Acknowledgments

H.Y. acknowledge funding support from the ASME Haythornthwaite Research Initiation Grant Award.

References

- [1] M. A. Wyczalkowski, Z. Chen, B. A. Filas, V. D. Varner, and L. A. Taber, “Computational Models for Mechanics of Morphogenesis,” vol. 152, no. Part C, pp. 132–152, 2012.

- [2] M. S. STEINBERG, “Reconstruction of tissues by dissociated cells. Some morphogenetic tissue movements and the sorting out of embryonic cells may have a common explanation.,” *Science*, vol. 141, no. 3579, pp. 401–8, Aug. 1963.
- [3] A. F. M. Marée, P. Hogeweg, and A. F. M. Mare, “How amoeboids self-organize into a fruiting body: Multicellular coordination in *Dictyostelium discoideum*,” *Proc. Natl. Acad. Sci.*, vol. 98, no. 7, pp. 3879–3883, 2001.
- [4] L. Geris, Ed., *Computational Modeling in Tissue Engineering*. 2013.
- [5] E. H. Davidson, J. P. Rast, P. Oliveri, A. Ransick, C. Calestani, C. Yuh, T. Minokawa, G. Amore, V. Hinman, C. Arenas-Mena, O. Otim, C. T. Brown, C. B. Livi, P. Y. Lee, R. Revilla, A. G. Rust, Z. jun Pan, M. J. Schilstra, P. J. C. Clarke, M. I. Arnone, L. Rowen, R. A. Cameron, D. R. McClay, L. Hood, and H. Bolouri, “A genomic regulatory network for development.,” *Science*, vol. 295, no. 2002, pp. 1669–1678, 2002.
- [6] L. V. Beloussov, *The Dynamic Architecture of a Developing Organism: An Interdisciplinary Approach to the Development of Organisms*. 1998.
- [7] L. A. Taber, “Theoretical study of Beloussov’s hyper-restoration hypothesis for mechanical regulation of morphogenesis,” *Biomech. Model. Mechanobiol.*, vol. 7, pp. 427–441, 2008.
- [8] J. Howard, S. W. Grill, and J. S. Bois, “Turing’s next steps: the mechanochemical basis of morphogenesis,” *Nat Rev Mol Cell Biol*, vol. 12, no. 6, pp. 392–398, 2011.
- [9] C. M. Lo, H. B. Wang, M. Dembo, and Y.-L. Wang, “Cell movement is guided by the rigidity of the substrate,” *Biophys. J.*, vol. 79, pp. 144–152, 2000.

- [10] P. Uttayarat, G. K. Toworfe, F. Dietrich, P. I. Lelkes, and R. J. Composto, "Topographic guidance of endothelial cells on silicone surfaces with micro- to nanogrooves: Orientation of actin filaments and focal adhesions," *J. Biomed. Mater. Res. Part A*, vol. 75A, no. 3, pp. 668–680, 2005.
- [11] E. T. Den Braber, J. E. De Ruijter, L. A. Ginsel, A. F. Von Recum, and J. A. Jansen, "Quantitative analysis of fibroblast morphology on microgrooved surfaces with various groove and ridge dimensions," *Biomaterials*, vol. 17, no. 21, pp. 2037–2044, 1996.
- [12] C. Oakley, N. A. F. Jaeger, and D. M. Brunette, "Sensitivity of fibroblasts and their cytoskeletons to substratum topographies: Topographic guidance and topographic compensation by micromachined grooves of different dimensions," *Exp. Cell Res.*, vol. 234, no. 2, pp. 413–424, 1997.
- [13] F. van Delft, F. C. van den Heuvel, W. A. Loesberg, J. T. Riet, P. Schon, C. G. Figdor, S. Speller, J. van Loon, X. F. Walboomers, J. A. Jansen, F. C. M. J. M. Van Delft, F. C. Van Den Heuvel, and P. Scho, "Manufacturing substrate nano-grooves for studying cell alignment and adhesion," 2008, vol. 85, pp. 1362–1366.
- [14] E. T. denBraber, J. E. deRuijter, L. A. Ginsel, A. F. vonRecum, and J. A. Jansen, "Quantitative analysis of fibroblast morphology on microgrooved surfaces with various groove and ridge dimensions," *Biomaterials*, vol. 17, no. 21, pp. 2037–2044, 1996.
- [15] P. Clark, P. Connolly, A. S. G. Curtis, J. A. T. Dow, C. D. W. Wilkinson, P. Clarke, and P. Connolly, "Topographical Control of Cell Behavior .2. Multiple Grooved Substrata," *Development*, vol. 108, no. 4, pp. 635–644, 1990.

- [16] J. S. Harunaga and K. M. Yamada, “Cell-matrix adhesions in 3D,” *Matrix Biol.*, vol. 30, no. 7–8, pp. 363–368, 2011.
- [17] F. Grinnell, C.-H. Ho, E. Tamariz, D. J. Lee, and G. Skuta, “Dendritic Fibroblasts in Three-dimensional Collagen Matrices,” *Mol. Biol. Cell*, vol. 14, no. 2, pp. 384–395, Feb. 2003.
- [18] F. Grinnell, “Fibroblast biology in three-dimensional collagen matrices,” *Trends Cell Biol.*, vol. 13, no. 5, pp. 264–269, 2003.
- [19] B. M. Baker and C. S. Chen, “Deconstructing the third dimension - how 3D culture microenvironments alter cellular cues,” *J. Cell Sci.*, vol. 125, no. July, pp. 3015–3024, 2012.
- [20] A. D. Doyle, F. W. Wang, K. Matsumoto, and K. M. Yamada, “One-dimensional topography underlies three-dimensional fibroblast cell migration,” *J. Cell Biol.*, vol. 184, no. 4, pp. 481–490, 2009.
- [21] C. S. Chen, J. Tan, and J. Tien, “MECHANOTRANSDUCTION AT CELL-MATRIX AND CELL-CELL CONTACTS,” *Annu. Rev. Biomed. Eng.*, vol. 6, no. 1, pp. 275–302, 2004.
- [22] K. K. Parker, A. L. Brock, C. Brangwynne, R. J. Mannix, N. Wang, E. Ostuni, N. A. Geisse, J. C. Adams, G. M. Whitesides, and D. E. Ingber, “Directional control of lamellipodia extension by constraining cell shape and orienting cell tractional forces,” *FASEB J*, vol. 16, no. 10, pp. 1195–1204, 2002.
- [23] A. Grosberg, P.-L. Kuo, C.-L. Guo, N. A. Geisse, M. A. Bray, W. J. Adams, S. P. Sheehy, and K. K. Parker, “Self-Organization of Muscle Cell Structure and Function,” *PLoS Comput Biol*, vol. 7, no. 2, p. e1001088, 2011.

- [24] K. K. Parker, J. Tan, C. S. Chen, and L. Tung, “Myofibrillar architecture in engineered cardiac myocytes,” *Circ Res*, vol. 103, no. 4, pp. 340–342, 2008.
- [25] M. A. Bray, S. P. Sheehy, and K. K. Parker, “Sarcomere alignment is regulated by myocyte shape,” *Cell Motil. Cytoskeleton*, vol. 65, pp. 641–651, 2008.
- [26] M. D. Onsum and C. V Rao, “Calling heads from tails : the role of mathematical modeling in understanding cell polarization,” pp. 74–81, 2009.
- [27] R. Wedlich-Soldner, S. Altschuler, L. Wu, and R. Li, “Spontaneous cell polarization through actomyosin-based delivery of the Cdc42 GTPase,” *Science (80-.)*, vol. 299, no. 5610, pp. 1231–1235, 2003.
- [28] J. Satulovsky, R. Lui, and Y. Wang, “Exploring the Control Circuit of Cell Migration by Mathematical Modeling,” *Biophys. J.*, vol. 94, no. 9, pp. 3671–3683, 2008.
- [29] A. F. M. Marée, A. Jilkin, A. Dawes, V. A. Grieneisen, and L. Edelstein-Keshet, *Polarization and movement of keratocytes: A multiscale modelling approach*, vol. 68, no. 5. 2006.
- [30] I. L. Novak, B. M. Slepchenko, A. Mogilner, and L. M. Loew, “Cooperativity between cell contractility and adhesion,” *Phys. Rev. Lett.*, vol. 93, no. 26 I, p. 268109, 2004.
- [31] X. Zeng and S. Li, “Multiscale modeling and simulation of soft adhesion and contact of stem cells,” *J. Mech. Behav. Biomed. Mater.*, vol. 4, no. 2, pp. 180–189, 2011.
- [32] V. S. Deshpande, R. M. McMeeking, and A. G. Evans, “A bio-chemo-mechanical model for cell contractility,” *Proc. Natl. Acad. Sci. U. S. A.*, vol. 103, no.

38, pp. 14015–14020, 2006.

[33] S. Walcott and S. X. Sun, “A mechanical model of actin stress fiber formation and substrate elasticity sensing in adherent cells,” *Proc. Natl. Acad. Sci. U. S. A.*, vol. 107, no. 17, pp. 7757–7762, 2010.

[34] J. Kang, R. L. Steward, Y. T. Kim, R. S. Schwartz, P. R. LeDuc, and K. M. Puskar, “Response of an actin filament network model under cyclic stretching through a coarse grained Monte Carl approach,” *J. Theor. Biol.*, vol. 274, no. 1, pp. 109–119, 2011.

[35] A. Pathak, V. S. Deshpande, R. M. McMeeking, and A. G. Evans, “The simulation of stress fibre and focal adhesion development in cells on patterned substrates,” *J. R. Soc. Interface*, vol. 5, pp. 507–524, 2008.

[36] H. Yuan, B. Marzban, and K. K. Parker, “Myofibrils in Cardiomyocytes Tend to Assemble Along the Maximal Principle Stress Directions,” *J Biomech Eng*, vol. doi: 10.11, 2017.

[37] M. L. McCain, H. Lee, Y. Aratyn-Schaus, A. G. Kléber, and K. K. Parker, “Cooperative coupling of cell-matrix and cell–cell adhesions in cardiac muscle,” *Proc. Natl. Acad. Sci.*, vol. 109, no. 25, pp. 9881–9886, 2012.

[38] Y. Aratyn-Schaus, F. S. Pasqualini, H. Yuan, M. L. McCain, G. J. C. Ye, S. P. Sheehy, P. H. Campbell, and K. K. Parker, “Coupling primary and stem cell–derived cardiomyocytes in an in vitro model of cardiac cell therapy,” *J. Cell Biol.*, vol. February 8, 2016.

[39] A. Chopra, E. Tabdanov, H. Patel, P. a Janmey, and J. Y. Kresh, “Cardiac myocyte remodeling mediated by N-cadherin-dependent mechanosensing,” *Am. J.*

- Physiol. - Hear. Circ. Physiol.*, vol. 300, no. 4, pp. H1252–H1266, Apr. 2011.
- [40] J. Y. Sim, J. Moeller, K. C. Hart, D. Ramallo, V. Vogel, A. R. Dunn, W. J. Nelson, and B. L. Pruitt, “Spatial distribution of cell-cell and cell-ECM adhesions regulates force balance while maintaining E-cadherin molecular tension in cell pairs,” *Mol. Biol. Cell*, vol. 26, no. 13, pp. 2456–2465, 2015.
- [41] C. G. Rolli, H. Nakayama, K. Yamaguchi, J. P. Spatz, R. Kemkemer, and J. Nakanishi, “Switchable adhesive substrates: Revealing geometry dependence in collective cell behavior,” *Biomaterials*, vol. 33, no. 8, pp. 2409–2418, 2012.
- [42] D. T. Tambe, C. C. Hardin, T. E. Angelini, K. Rajendran, C. Y. Park, X. Serra-Picamal, E. H. Zhou, M. H. Zaman, J. P. Butler, D. A. Weitz, J. J. Fredberg, and X. Trepat, “Collective cell guidance by cooperative intercellular forces,” *Nat. Mater.*, vol. 10, no. 6, pp. 469–75, 2011.
- [43] M. Tahersima and P. Tikalsky, “Finite element modeling of hydration heat in a concrete slab-on-grade floor with limestone blended cement,” *Constr. Build. Mater.*, vol. 154, pp. 44–50, 2017.
- [44] A. Mehrvarz, M. J. Khodaei, W. Clark, and N. Jalili, “Modeling and Dynamics Analysis of a Beam-Hoverboard Self-Transportation System,” no. 51913. p. V003T32A008, 2018.
- [45] M. J. Khodaei, A. Mehrvarz, N. Candelino, and N. Jalili, “Theoretical and Experimental Analysis of Coupled Flexural-Torsional Vibrations of Rotating Beams,” no. 51913. p. V003T42A004, 2018.
- [46] S. Jafarzadeh and M. Kadkhodaei, “Finite element simulation of ferromagnetic shape memory alloys using a revised constitutive model,” *J. Intell. Mater. Syst.*

- Struct.*, vol. 28, no. 19, pp. 2853–2871, 2017.
- [47] S. Jafarzadeh, Z. Chen, and F. Bobaru, “Peridynamic Modeling of Repassivation in Pitting Corrosion of Stainless Steel,” *Corrosion*, vol. 74, no. 4, pp. 393–414, 2018.
- [48] R. Ghaffarivardavagh, J. Nikolajczyk, R. Glynn Holt, S. Anderson, and X. Zhang, “Horn-like space-coiling metamaterials toward simultaneous phase and amplitude modulation,” *Nat. Commun.*, vol. 9, no. 1, 2018.
- [49] P. Li *et al.*, “Acoustic separation of circulating tumor cells,” *Proc. Natl. Acad. Sci.*, vol. 112, no. 16, pp. 4970–4975, 2015.

CHAPTER 5 :

Conclusions and Future Work

Conclusions

An efficient and robust computational biomechanics model and software platform has been developed to simulate the dynamics of living cells at the whole-cell level. Specific biomechanics phenomenon including cell crawling and morphogenesis of cell monolayer tissues has been studied using the computational model. It has been shown that mechanical and external forces play a key role in biological cells and their motility using this bottom up mathematical model.

Nowadays, there are plenty of the real world systems that researchers need to replicate them digitally. This works provides an insight to the digital twin of the biological cell models. From the technological point of view, this project will pave the way for a deeper understanding of the mechanobiochemical mechanisms in cell-microenvironment interactions that regulate microtissue morphogenesis, enabling computer-aided rational design of the cell microenvironment in tissue engineering such as 3D bioprinting.

Future Work

The developed computational model can be applied to different cells types (e.g., fibroblasts, endothelial cells, smooth muscle cells, and neurons). To further extend the

boundaries of this current research, the following research directions are recommended:

- Extending the model to 3Dimensional model and mimic the 3D tissue in vivo.
- Conducting a full parameter space search

Extending the Model to 3Dimensional Model

In order to mimic the 3D tissue in vivo, the model should be utilized and be formulated for the 3Dimensional simulation. In 3D, remeshing is the most expensive computational. Using meshless methods can be useful to deal with computational cost of the remeshing. For future direction we propose develop a 3Dimensional finite element-based computational model and parallelized software toolbox to simulate cells and ECM so that microtissues in millimeter scales can be simulated with high fidelity. This computational model will be used to elucidate and understand the morphological pattern formations in the microtissues that consist of many cells.

Parameter space search

The parameter space and mathematical formulations will be searched to identify the sub-spaces in which the computational model predicts characteristic behaviors of each type of differentiated cells, as well as the characteristic microscale morphologies of each type of tissues (e.g., bundling in muscle tissue, branching in nerve tissue, polarization in epithelial tissue).

The genetic algorithm will be used to estimate the parameter values and search for mathematical formulations with which the behavior of the model best matches that of experiments. With automated high-resolution life-cell imaging techniques, large amounts of experimental data are being collected in cell biology labs worldwide. To accelerate the search, the numerical program of this optimization in a large multidimensional space will be parallelized and performed on the high-performance computers with hundreds of computer nodes. As shown in the flowchart in Fig. 1, different sets of model parameters and model equations are used as the input set. The first generation of the sets will be evaluated by their fitness and each computer node runs calculations for each individual in a population by using distributed parallel computing. Characteristic of cell migration, such as cell shape, cytoskeleton architecture, migration speed, etc., will be extracted from the simulations and used to compare with the metrics calculated from the experimental observations. Following that, if the convergence criteria is met, the search will stop, and if not, the calculation will be continued by producing the second generation using evolutionary methods; for example, crossover, mutation, etc. The second generation will be evaluated according to their fitness and so on. The proposed model allows one to identify which set of parameters and equations (i.e., assumptions or hypotheses) will match the specific cell migration behavior.

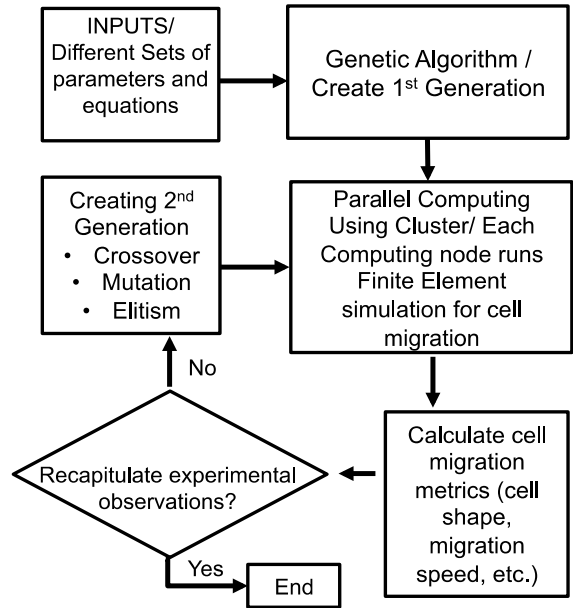


Figure 1. Flowchart of the genetic algorithm for parameter space search.

The model and the computer simulation program, once developed and validated, will be used in computer-aided design in tissue engineering. For example, it will be used to design suitable biomaterials with optimal mechanical properties, the optimal topology of ECM, and the 3D spatial placement of cells, to facilitate microtissue formation. In tissue-engineering applications, biological and chemical parameters are frequently considered, while the equally important physical/mechanical design variables have often been neglected. For a rational design of tissue engineering, however, all variables influencing cell function and tissue morphogenesis must be considered. This proposed computational model on microtissue formation will enable the integration of chemical, mechanical, and topographical aspects of the problem and can have a powerful impact on the rational design in 3D bioprinting.

APPENDICES

Appendix A (Major subroutines)

a_para_basic.m

Input variables for the model parameters.

a_driver_durotaxis.m

This driver will set the other required parameters for the durotaxis simulation and within the driver we can either choose to run a simulation or plot the previous simulation results. Therefore the driver calls either *a_multicellular_system.m* or the *plot_simulation_results.m*. Note, that there are different drivers for different scenarios.

a_multicellular_system.m

This is the main function of the program, it will call the initialization subroutine and starts the time integration loop, follows the detailed flowchart in Figure 3, and calls for the solvers. It will end the simulation whenever the simulation time reaches.

calc_delta_t.m

This subroutine calculates the time step dt .

The algorithm adopts an adjustable time step to make sure that the time integration is stable. It estimates the maximum possible time step for numerical integration based on the following two criteria:

1. $dt < 1/10 * \min\{\text{time scales of decay for all time-dependent variables}\}$
2. $dt < (1/4 * (\text{smallest element size})^2 / \min\{\text{Diffusion constants}\})$

After the estimation if the input time step is bigger than the estimated time step. It assigns the estimated time step to the time step variable dt to make sure that we have an stable time integration.

a_multicellular_initialization.m

This subroutine initializes the matrix/tensors/vectors we are using for the finite element simulation. It will call following subroutines:

mesh_a_cell_m.m

This subroutine is for discretizing the 2D cell domain based on the initial cell shape and the element type. Based on the *para.initial_cell_shape* input, we can switch between several cell shapes and element type. This algorithm also returns the edge segments of the domain.

mesh_find_and_sort_cell_edge.m

The input for this algorithm is the nodal coordinates and the connectivity matrix from the *mesh_a_cell_m.m* subroutine. And the output is the edge segments.

mesh_brand_new_remeshing.m

this subroutine is for the automatic mesh generation. It creates initial distribution in bounding box, add more points near the edge, add some random noise to the coordinates in case the algorithm does not converge well, remove points outside the region, applies Delaunay triangulation to create elements.

mesh_remove_narrow_membrane_tub.m

remove narrow and tube elements. This happens when cells become too narrow at some zones.

mesh_fix_delaunay_mesh.m

this algorithm fixes the meshes after the Delaunay triangulation. Several problems may occur after the default Delaunay triangulation: multiple loops, interior nodes come to edge, and also check if multiple loops exist due to Delaunay triangulation, keep the biggest one.

mesh_clear_singular_node.m

This algorithm removes the singular nodes. In a regular good topology, simple topology, each edge node has two edge segments. Singular nodes have 4 edge segments; we use this rule to find singular nodes

mesh_find_cell_edge_only.m

This subroutine assumes the element nodal numbering is counter clockwise.

mesh_find_edge_normal.m

Finds the normal to the boundary/edges of cell on the nodes.

mesh_Laplacian_smoothing.m

Without changing the connectivity matrix of mesh, optimize the nodal positions to obtain high quality mesh.

apply_zero_FA_condition.m

This subroutine applies adhesive island boundary condition by setting the focal adhesion of those region of the substrate equal to zero.

update_microtubule.m

This subroutine updates the vector associated with microtubule.

update_Stress_Fiber.m

This subroutine updates the stress fiber based on the model.

solver_reaction_diffusion.m

This subroutine solves the system of equations resulted from the finite element model of the reaction diffusion equation. It also has option to switch for different type of the elements.

solver_elasticity.m

This is a two-dimensional finite element model for solving the elasticity and finding the displacement. It's include assembly of the mass and stiffness matrix and solving the system of equations.

solver_rate_equation.m

This subroutine is for solving the rate equation. For example, the focal adhesion rate equation.

solver_FEA_K_M.m

This solver pre-calculates the mass (M) and stiffness (K) matrix to avoid calculating that in each time steps.

update_cc_adhesion_bond.m

updates the cell-cell adhesion bond in each iteration.

calc_cell_retraction.m

calculate retraction of the cell using the Eq. (12)

get_cell_neighbors.m

update the neighbors cell list based on a cut off distance.

calc_P_source.m

this subroutine is for calculating the source term of the reaction diffusion equation for the protrusion.

update_variables_after_growth.m

This subroutine updates the variables after the growth happened.

update_variables_after_remeshing_m.m

This subroutine transfers the field variables to the new sets of elements after remeshing.

calc_cell_growth_node_based.m

this subroutine updates the protrusion displacement of the cells based on Eq. (11)

Appendix B (Variables)

The parameter values for the simulations will be chosen from the available experimental data in the literature, the rest of the parameters will be chosen in a fashion to obtain similar results to experimental studies in the literature. Following are the parameter values used for the simulations in this study unless specifically mentioned.

Table 1. Parameter used in the simulations. Some of the variables derived from the literature and the rest are the estimated parameter.

<i>Symbol</i>	<i>Variable</i>	<i>Value</i>
A_c	Cell initial area	$900 \mu\text{m}^2$
A_{max}	Cell area upper limit	$1800 \mu\text{m}^2$
A_{min}	Cell area lower limit	$110 \mu\text{m}^2$
V_{cell}	Cell volume	$2000 \mu\text{m}^3$
E	Young modulus of the cell	4kPa
ν	Poisson ration of the cell	0.3
k_{ECM}	Equivalent spring constant of the substrate	$0.5 \text{ kPa} / \mu\text{m}$
σ_{c0}	Baseline contractility	0.6kPa
σ_{c1}	Retraction signal-associated contractility	0kPa
σ_{cf}	Stress fiber-associated contractility	2kPa
σ_m	Model parameter for stress fiber	2kPa
K_{on}^S	Stress fiber activation rate	0.03
K_{off}^S	Stress fiber deactivation rate	0.03
$k_{\text{FA}}^{\text{max}}$	Maximal stiffness corresponds to maximum focal adhesion	1
ρ_a	Average density of the total amount of bound and unbound focal adhesion proteins	0.16
K_0^p	Rate constants for the spontaneous focal adhesion formation	0.03
K_ξ^p	Rate constants for protrusion signal-dependent	0
K_{off}^p	Decay rate constant for focal adhesion formation	0.03
K_T^p	Rate constants Stress-mediated focal adhesion formation	0
K_M^p	Rate constant for auto-activation focal adhesion formation	0.1
T_0	Model parameter for the focal adhesion	0.36
n_4	Model parameter for the focal adhesion	2
D_ζ	Diffusivity constant of retraction active proteins in membrane	0.5
D_ξ	Diffusivity constant of protrusion active proteins in membrane	0.5
ξ_a	Total concentrations of both active and inactive form of the protrusion signal	0.1
ζ_a	Total concentrations of both active and inactive form of the retraction signal	0.1
K_0^ξ	Rate constants for the spontaneous activation of protrusion signals	0.14
K_T^ξ	Rate constants for the stress-mediated activation of protrusion signals	0.45
K_M^ξ	Rate constants for the auto-activation of protrusion signals	0.1
ξ_0	Model parameters describing the auto-inhibition	0.1

ζ_0	Model parameters describing the auto-inhibition	0.1
K_{off}^ξ	Decay constant for the deactivation of the protrusion signals	0.14
R_ξ	Strength of random noise for protrusion signals	0.0001
K_0^ζ	Rate constants for the spontaneous activation of retraction signal	0.14
K_{off}^ζ	Decay constant for the deactivation of the retraction signal	0.07
n_1	Model parameter for protrusion RD model	4
n_2	Model parameter for protrusion RD model	2
n_3	Model parameter for retraction RD model	4
c_p	Model parameter for cell growth	0.25
ξ_p	Protrusion threshold for cell growth	0.3
c_r	Model Parameter for retraction velocity	0.01
K_M	Rate constant for the microtubule model	0.02
c_e	Model parameter for the microtubule vector	1
n	Model parameter for microtubule	4

BIBLIOGRAPHY

- Allena, R., Scianna, M., & Preziosi, L. (2016). A Cellular Potts Model of single cell migration in presence of durotaxis. *Mathematical Biosciences*, 275, 57–70.
<https://doi.org/10.1016/j.mbs.2016.02.011>
- Altschuler, S. J., Angenent, S. B., Wang, Y., & Wu, L. F. (2008). On the spontaneous emergence of cell polarity. *Nature*, 454(7206), 886–889.
https://doi.org/http://www.nature.com/nature/journal/v454/n7206/supinfo/nature07119_S1.html
- Aratyn-Schaus, Y., Pasqualini, F. S., Yuan, H., McCain, M. L., Ye, G. J. C., Sheehy, S. P., ... Parker, K. K. (2016). Coupling primary and stem cell-derived cardiomyocytes in an in vitro model of cardiac cell therapy. *The Journal of Cell Biology*, February 8. <https://doi.org/10.1083/jcb.201508026>
- Baker, B. M., & Chen, C. S. (2012). Deconstructing the third dimension - how 3D culture microenvironments alter cellular cues. *Journal of Cell Science*, 125(July), 3015–3024. <https://doi.org/10.1242/jcs.079509>
- Barnhart, E. L., Lee, K. C., Keren, K., Mogilner, A., & Theriot, J. A. (2011). An adhesion-dependent switch between mechanisms that determine motile cell shape. *PLoS Biology*, 9(5). <https://doi.org/10.1371/journal.pbio.1001059>
- Belousov, L. V. (1998). *The Dynamic Architecture of a Developing Organism: An Interdisciplinary Approach to the Development of Organisms*.
- Borau, C., Kamm, R. D., & García-Aznar, J. M. (2011). Mechano-sensing and cell migration: A 3D model approach. *Physical Biology*, 8(6).

<https://doi.org/10.1088/1478-3975/8/6/066008>

- Borau, C., Kamm, R. D., & García-Aznar, J. M. (2014). A time-dependent phenomenological model for cell mechano-sensing. *Biomechanics and Modeling in Mechanobiology*, *13*(2), 451–462. <https://doi.org/10.1007/s10237-013-0508-x>
- Bray, M. A., Sheehy, S. P., & Parker, K. K. (2008). Sarcomere alignment is regulated by myocyte shape. *Cell Motility and the Cytoskeleton*, *65*, 641–651. <https://doi.org/10.1002/cm.20290>
- Breckenridge, M. T., Desai, R. A., Yang, M. T., Fu, J., & Chen, C. S. (2014). Substrates with engineered step changes in rigidity induce traction force polarity and durotaxis. *Cellular and Molecular Bioengineering*, *7*(1), 26–34. <https://doi.org/10.1007/s12195-013-0307-6>
- Brock, A., Chang, E., Ho, C. C., LeDuc, P., Jiang, X., Whitesides, G. M., & Ingber, D. E. (2003). Geometric determinants of directional cell motility revealed using microcontact printing. *Langmuir*, *19*(5), 1611–1617. <https://doi.org/10.1021/la026394k>
- Chen, C. S. (2008). Mechanotransduction - a field pulling together? *Journal of Cell Science*, *121*(20), 3285–3292. <https://doi.org/10.1242/jcs.023507>
- Chen, C. S., Tan, J., & Tien, J. (2004). MECHANOTRANSDUCTION AT CELL-MATRIX AND CELL-CELL CONTACTS. *Annual Review of Biomedical Engineering*, *6*(1), 275–302. <https://doi.org/doi:10.1146/annurev.bioeng.6.040803.140040>
- Chopra, A., Tabdanov, E., Patel, H., Janmey, P. a, & Kresh, J. Y. (2011). Cardiac myocyte remodeling mediated by N-cadherin-dependent mechanosensing.

American Journal of Physiology - Heart and Circulatory Physiology, 300(4), H1252–H1266. <https://doi.org/10.1152/ajpheart.00515.2010>

Clark, P., Connolly, P., Curtis, A. S. G., Dow, J. A. T., Wilkinson, C. D. W., Clarke, P., & Connolly, P. (1990). Topographical Control of Cell Behavior .2. Multiple Grooved Substrata. *Development*, 108(4), 635–644.

Cohen, O., & Safran, S. A. (2016). Elastic interactions synchronize beating in cardiomyocytes. *Soft Matter*, 12(28), 6088–6095. <https://doi.org/10.1039/C6SM00351F>

Danuser, G., Allard, J., & Mogilner, A. (2013). Mathematical modeling of eukaryotic cell migration: insights beyond experiments. *Annu Rev Cell Dev Biol*, 29, 501–528. <https://doi.org/10.1146/annurev-cellbio-101512-122308>

Davidson, E. H., Rast, J. P., Oliveri, P., Ransick, A., Caestani, C., Yuh, C., ... Bolouri, H. (2002). A genomic regulatory network for development. *Science (New York, N.Y.)*, 295(2002), 1669–1678. <https://doi.org/10.1126/science.1069883>

del Rio, A., Perez-jimenez, R., Liu, R., Roca-Cusachs, P., Fernandez, J. M., & Sheetz, M. P. (2009). Stretching Single Talin Rod Molecules Activates Vinculin Binding. *Science*, 323(5914), 638–641. <https://doi.org/10.1126/science.1162912>

Den Braber, E. T., De Ruijter, J. E., Ginsel, L. A., Von Recum, A. F., & Jansen, J. A. (1996). Quantitative analysis of fibroblast morphology on microgrooved surfaces with various groove and ridge dimensions. *Biomaterials*, 17(21), 2037–2044. [https://doi.org/10.1016/0142-9612\(96\)00032-4](https://doi.org/10.1016/0142-9612(96)00032-4)

denBraber, E. T., deRuijter, J. E., Ginsel, L. A., vonRecum, A. F., & Jansen, J. A.

- (1996). Quantitative analysis of fibroblast morphology on microgrooved surfaces with various groove and ridge dimensions. *Biomaterials*, 17(21), 2037–2044.
- Deshpande, V. S., McMeeking, R. M., & Evans, A. G. (2006). A bio-chemo-mechanical model for cell contractility. *Proceedings of the National Academy of Sciences of the United States of America*, 103(38), 14015–14020. Journal Article. <https://doi.org/10.1073/pnas.0605837103>
- Devreotes, P., & Horwitz, A. R. (2015). Signaling networks that regulate cell migration. *Cold Spring Harb Perspect Biol*, 7(8), a005959.
- Dormann, D., & Weijer, C. J. (2006). Imaging of cell migration. *EMBO Journal*, 25(15), 3480–3493. <https://doi.org/10.1038/sj.emboj.7601227>
- Doyle, A. D., Wang, F. W., Matsumoto, K., & Yamada, K. M. (2009). One-dimensional topography underlies three-dimensional fibroblast cell migration. *Journal of Cell Biology*, 184(4), 481–490. <https://doi.org/10.1083/jcb.200810041>
- Engler, A. J., Sen, S., Sweeney, H. L., & Discher, D. E. (2006). Matrix elasticity directs stem cell lineage specification. *Cell*, 126(4), 677–689. <https://doi.org/10.1016/j.cell.2006.06.044>
- Forgacs, G., & Newman, S. A. (2005). *Biological Physics of the Developing Embryo*. Cambridge: Cambridge University Press. <https://doi.org/DOI:10.1017/CBO9780511755576>
- Franck, C., Maskarinec, S. A., Tirrell, D. A., & Ravichandran, G. (2011). Three-Dimensional Traction Force Microscopy: A New Tool for Quantifying Cell-Matrix Interactions. *PLoS ONE*, 6(3), e17833. <https://doi.org/10.1371/journal.pone.0017833>

- Gao, H., Qian, J., & Chen, B. (2011, September). Probing mechanical principles of focal contacts in cell–matrix adhesion with a coupled stochastic–elastic modelling framework. *Journal of the Royal Society Interface*.
<https://doi.org/10.1098/rsif.2011.0157>
- Geris, L. (Ed.). (2013). *Computational Modeling in Tissue Engineering*.
- Ghaffarivardavagh, R., Nikolajczyk, J., Glynn Holt, R., Anderson, S., & Zhang, X. (2018). Horn-like space-coiling metamaterials toward simultaneous phase and amplitude modulation. *Nature Communications*, *9*(1).
<https://doi.org/10.1038/s41467-018-03839-z>
- Ghibaudo, M., Saez, A., Trichet, L., Xayaphoummine, A., Browaeys, J., Silberzan, P., ... Ladoux, B. (2008). Traction forces and rigidity sensing regulate cell functions. *Soft Matter*, *4*(9), 1836–1843. <https://doi.org/10.1039/b804103b>
- Grinnell, F. (2003). Fibroblast biology in three-dimensional collagen matrices. *Trends in Cell Biology*, *13*(5), 264–269. [https://doi.org/10.1016/S0962-8924\(03\)00057-6](https://doi.org/10.1016/S0962-8924(03)00057-6)
- Grinnell, F., Ho, C.-H., Tamariz, E., Lee, D. J., & Skuta, G. (2003). Dendritic Fibroblasts in Three-dimensional Collagen Matrices. *Molecular Biology of the Cell*, *14*(2), 384–395.
- Grosberg, A., Kuo, P.-L., Guo, C.-L., Geisse, N. A., Bray, M. A., Adams, W. J., ... Parker, K. K. (2011). Self-Organization of Muscle Cell Structure and Function. *PLoS Comput Biol*, *7*(2), e1001088. <https://doi.org/10.1371/journal.pcbi.1001088>
- Harunaga, J. S., & Yamada, K. M. (2011). Cell-matrix adhesions in 3D. *Matrix Biology*, *30*(7–8), 363–368. <https://doi.org/10.1016/j.matbio.2011.06.001>
- Howard, J., Grill, S. W., & Bois, J. S. (2011). Turing’s next steps: the

- mechanochemical basis of morphogenesis. *Nat Rev Mol Cell Biol*, 12(6), 392–398.
- Iglesias, P. a., & Devreotes, P. N. (2012). Biased excitable networks: How cells direct motion in response to gradients. *Current Opinion in Cell Biology*, 24(2), 245–253. <https://doi.org/10.1016/j.ceb.2011.11.009>
- Isenberg, B. C., Dimilla, P. A., Walker, M., Kim, S., & Wong, J. Y. (2009). Vascular smooth muscle cell durotaxis depends on substrate stiffness gradient strength. *Biophysical Journal*, 97(5), 1313–1322. <https://doi.org/10.1016/j.bpj.2009.06.021>
- Jafarzadeh, S., Chen, Z., & Bobaru, F. (2018). Peridynamic Modeling of Repassivation in Pitting Corrosion of Stainless Steel. *Corrosion*, 74(4), 393–414. <https://doi.org/10.5006/2615>
- Jafarzadeh, S., & Kadkhodaei, M. (2017). Finite element simulation of ferromagnetic shape memory alloys using a revised constitutive model. *Journal of Intelligent Material Systems and Structures*, 28(19), 2853–2871. <https://doi.org/10.1177/1045389X17704064>
- Kang, J., Steward, R. L., Kim, Y. T., Schwartz, R. S., LeDuc, P. R., & Puskar, K. M. (2011). Response of an actin filament network model under cyclic stretching through a coarse grained Monte Carl approach. *Journal of Theoretical Biology*, 274(1), 109–119.
- Khodaei, M. J., Mehrvarz, A., Candelino, N., & Jalili, N. (2018). Theoretical and Experimental Analysis of Coupled Flexural-Torsional Vibrations of Rotating Beams. Retrieved from <http://dx.doi.org/10.1115/DSCC2018-9050>
- Kim, J. H., Serra-Picamal, X., Tambe, D. T., Zhou, E. H., Park, C. Y., Sadati, M., ...

- Fredberg, J. J. (2013). Propulsion and navigation within the advancing monolayer sheet. *Nature Materials*, *12*(9), 856–863. <https://doi.org/10.1038/nmat3689>
- Li, P., Mao, Z., Peng, Z., Zhou, L., Chen, Y., Huang, P.-H., ... Huang, T. J. (2015). Acoustic separation of circulating tumor cells. *Proceedings of the National Academy of Sciences*, *112*(16), 4970–4975. <https://doi.org/10.1073/pnas.1504484112>
- Li, S., Butler, P., Wang, Y., Hu, Y., Han, D. C., Usami, S., ... Chien, S. (2002). The role of the dynamics of focal adhesion kinase in the mechanotaxis of endothelial cells. *Proceedings of the National Academy of Sciences of the United States of America*, *99*(6), 3546–3551. <https://doi.org/10.1073/pnas.052018099>
- Lo, C. M., Wang, H. B., Dembo, M., & Wang, Y.-L. (2000). Cell movement is guided by the rigidity of the substrate. *Biophysical Journal*, *79*, 144–152.
- Marcq, P., Yoshinaga, N., & Prost, J. (2011). Rigidity sensing explained by active matter theory. *Biophysical Journal*, *101*(6), 26–29. <https://doi.org/10.1016/j.bpj.2011.08.023>
- Marée, A. F. M., Grieneisen, V. A., & Edelstein-Keshet, L. (2012). How cells integrate complex stimuli: The effect of feedback from phosphoinositides and cell shape on cell polarization and motility. *PLoS Computational Biology*, *8*(3). <https://doi.org/10.1371/journal.pcbi.1002402>
- Marée, A. F. M., Hogeweg, P., & Mare, A. F. M. (2001). How amoeboids self-organize into a fruiting body: Multicellular coordination in *Dictyostelium discoideum*. *Proceedings of the National Academy of Sciences*, *98*(7), 3879–3883.

- Marée, A. F. M., Jilkin, A., Dawes, A., Grieneisen, V. A., & Edelstein-Keshet, L. (2006). *Polarization and movement of keratocytes: A multiscale modelling approach. Bulletin of Mathematical Biology* (Vol. 68).
<https://doi.org/10.1007/s11538-006-9131-7>
- Marzban, B., Yi, X., & Yuan, H. (2018). A minimal mechanics model for mechanosensing of substrate rigidity gradient in durotaxis. *Biomechanics and Modeling in Mechanobiology*. <https://doi.org/10.1007/s10237-018-1001-3>
- Marzban, B., & Yuan, H. (2016). The effect of viscous force on the prediction of muscle contractility in biohybrid cantilever-based experiments. *Extreme Mechanics Letters*, 9, 342–346. <https://doi.org/10.1016/j.eml.2016.09.011>
- Marzban, B., & Yuan, H. (2017). The effect of thermal fluctuation on the receptor-mediated adhesion of a cell membrane to an elastic substrate. *Membranes*, 7(2).
<https://doi.org/10.3390/membranes7020024>
- McCain, M. L., Lee, H., Aratyn-Schaus, Y., Kléber, A. G., & Parker, K. K. (2012). Cooperative coupling of cell-matrix and cell–cell adhesions in cardiac muscle. *Proceedings of the National Academy of Sciences*, 109(25), 9881–9886.
<https://doi.org/10.1073/pnas.1203007109>
- McCain, M. L., Yuan, H., Pasqualini, F. S., Campbell, P. H., & Parker, K. K. (2014). Matrix elasticity regulates the optimal cardiac myocyte shape for contractility. *American Journal of Physiology. Heart and Circulatory Physiology*, 306(11), H1525-39. <https://doi.org/10.1152/ajpheart.00799.2013>
- Mehrvarz, A., Khodaei, M. J., Clark, W., & Jalili, N. (2018). Modeling and Dynamics Analysis of a Beam-Hoverboard Self-Transportation System. Retrieved from

<http://dx.doi.org/10.1115/DSCC2018-9048>

- Mitrossilis, D., Fouchard, J., Guiroy, A., Desprat, N., Rodriguez, N., Fabry, B., & Asnacios, A. (2009). Single-cell response to stiffness exhibits muscle-like behavior. *Proceedings of the National Academy of Sciences*, *106*(43), 18243–18248. <https://doi.org/10.1073/pnas.0903994106>
- Moreo, P., García-Aznar, J. M., & Doblaré, M. (2008). Modeling mechanosensing and its effect on the migration and proliferation of adherent cells. *Acta Biomaterialia*, *4*(3), 613–621. <https://doi.org/10.1016/j.actbio.2007.10.014>
- Mori, Y., Jilkine, A., & Edelstein-Keshet, L. (2008). Wave-pinning and cell polarity from a bistable reaction-diffusion system. *Biophysical Journal*, *94*(9), 3684–3697. <https://doi.org/10.1529/biophysj.107.120824>
- Nelson, C. M., Jean, R. P., Tan, J. L., Liu, W. F., Sniadecki, N. J., Spector, A. A., & Chen, C. S. (2005). Emergent patterns of growth controlled by multicellular form and mechanics. *Proceedings of the National Academy of Sciences of the United States of America*, *102*(33), 11594–11599.
- Novak, I. L., Slepchenko, B. M., Mogilner, A., & Loew, L. M. (2004). Cooperativity between cell contractility and adhesion. *Physical Review Letters*, *93*(26 D), 268109. <https://doi.org/10.1103/PhysRevLett.93.268109>
- Oakley, C., Jaeger, N. A. F., & Brunette, D. M. (1997). Sensitivity of fibroblasts and their cytoskeletons to substratum topographies: Topographic guidance and topographic compensation by micromachined grooves of different dimensions. *Experimental Cell Research*, *234*(2), 413–424.
- Onsum, M. D., & Rao, C. V. (2009). Calling heads from tails : the role of

mathematical modeling in understanding cell polarization, 74–81.

<https://doi.org/10.1016/j.ceb.2009.01.001>

Otsuji, M., Ishihara, S., Co, C., Kaibuchi, K., Mochizuki, A., & Kuroda, S. (2007). A mass conserved reaction-diffusion system captures properties of cell polarity.

PLoS Computational Biology, 3(6), 1040–1054.

<https://doi.org/10.1371/journal.pcbi.0030108>

Parker, K. K., Brock, A. L., Brangwynne, C., Mannix, R. J., Wang, N., Ostuni, E., ...

Ingber, D. E. (2002). Directional control of lamellipodia extension by constraining cell shape and orienting cell tractional forces. *Faseb J*, 16(10), 1195–1204. Journal Article.

Parker, K. K., Tan, J., Chen, C. S., & Tung, L. (2008). Myofibrillar architecture in engineered cardiac myocytes. *Circ Res*, 103(4), 340–342. Journal Article.

Pathak, A., Deshpande, V. S., McMeeking, R. M., & Evans, A. G. (2008). The simulation of stress fibre and focal adhesion development in cells on patterned substrates. *Journal of the Royal Society Interface*, 5, 507–524. Journal Article.

Plotnikov, S. V., Pasapera, A. M., Sabass, B., & Waterman, C. M. (2012). Force fluctuations within focal adhesions mediate ECM-rigidity sensing to guide directed cell migration. *Cell*, 151(7), 1513–1527.

<https://doi.org/10.1016/j.cell.2012.11.034>

Polacheck, W. J., German, A. E., Mammoto, A., Ingber, D. E., & Kamm, R. D. (2014). Mechanotransduction of fluid stresses governs 3D cell migration.

Proceedings of the National Academy of Sciences of the United States of America, 111(7), 2447–2452. <https://doi.org/10.1073/pnas.1316848111>

- Prentice-Mott, H. V., Meroz, Y., Carlson, A., Levine, M. A., Davidson, M. W., Irimia, D., ... Shah, J. V. (2016). Directional memory arises from long-lived cytoskeletal asymmetries in polarized chemotactic cells. *Proceedings of the National Academy of Sciences*, *113*(5), 201513289.
<https://doi.org/10.1073/pnas.1513289113>
- Rahman, A., Carey, S. P., Kraning-Rush, C. M., Goldblatt, Z. E., Bordeleau, F., Lampi, M. C., ... Reinhart-King, C. A. (2016). Vinculin regulates directionality and cell polarity in two- and three-dimensional matrix and three-dimensional microtrack migration. *Molecular Biology of the Cell*, *27*(9), 1431–1441.
<https://doi.org/10.1091/mbc.E15-06-0432>
- Ridley, A. J., Schwartz, M. a, Burridge, K., Firtel, R. a, Ginsberg, M. H., Borisy, G., ... Horwitz, A. R. (2003). Cell migration: integrating signals from front to back. *Science (New York, N.Y.)*, *302*(5651), 1704–1709.
<https://doi.org/10.1126/science.1092053>
- Rolli, C. G., Nakayama, H., Yamaguchi, K., Spatz, J. P., Kemkemer, R., & Nakanishi, J. (2012). Switchable adhesive substrates: Revealing geometry dependence in collective cell behavior. *Biomaterials*, *33*(8), 2409–2418.
<https://doi.org/10.1016/j.biomaterials.2011.12.012>
- Satulovsky, J., Lui, R., & Wang, Y. (2008). Exploring the Control Circuit of Cell Migration by Mathematical Modeling. *Biophysical Journal*, *94*(9), 3671–3683.
<https://doi.org/http://dx.doi.org/10.1529/biophysj.107.117002>
- Sheetz, M. P., & Dai, J. (1996). Modulation of membrane dynamics and cell motility by membrane tension. *Trends in Cell Biology*, *6*(3), 85–89.

[https://doi.org/10.1016/0962-8924\(96\)80993-7](https://doi.org/10.1016/0962-8924(96)80993-7)

Sheetz, M. P., Felsenfeld, D. P., & Galbraith, C. G. (1998). Cell migration : regulation of force on extracellular-matrix-integrin complexes. *Trends in Cell Biology*, 8(97), 51–54. <https://doi.org/S0962892497012166> [pii]

Sim, J. Y., Moeller, J., Hart, K. C., Ramallo, D., Vogel, V., Dunn, A. R., ... Pruitt, B. L. (2015). Spatial distribution of cell-cell and cell-ECM adhesions regulates force balance while maintaining E-cadherin molecular tension in cell pairs. *Molecular Biology of the Cell*, 26(13), 2456–2465. <https://doi.org/10.1091/mbc.E14-12-1618>

STEINBERG, M. S. (1963). Reconstruction of tissues by dissociated cells. Some morphogenetic tissue movements and the sorting out of embryonic cells may have a common explanation. *Science (New York, N.Y.)*, 141(3579), 401–408.

Taber, L. A. (2008). Theoretical study of Belousov’s hyper-restoration hypothesis for mechanical regulation of morphogenesis. *Biomechanics and Modeling in Mechanobiology*, 7, 427–441. <https://doi.org/10.1007/s10237-007-0106-x>

Tahersima, M., & Tikalsky, P. (2017). Finite element modeling of hydration heat in a concrete slab-on-grade floor with limestone blended cement. *Construction and Building Materials*, 154, 44–50.
<https://doi.org/10.1016/j.conbuildmat.2017.07.176>

Tambe, D. T., Croutelle, U., Trepate, X., Park, C. Y., Kim, J. H., Millet, E., ... Fredberg, J. J. (2013). Monolayer Stress Microscopy: Limitations, Artifacts, and Accuracy of Recovered Intercellular Stresses. *PLoS ONE*, 8(2).
<https://doi.org/10.1371/journal.pone.0055172>

- Tambe, D. T., Hardin, C. C., Angelini, T. E., Rajendran, K., Park, C. Y., Serrapicamal, X., ... Trepap, X. (2011). Collective cell guidance by cooperative intercellular forces. *Nature Materials*, *10*(6), 469–475.
<https://doi.org/10.1038/nmat3025>
- Twiss, F., & De Rooij, J. (2013). Cadherin mechanotransduction in tissue remodeling. *Cellular and Molecular Life Sciences*, *70*(21), 4101–4116.
<https://doi.org/10.1007/s00018-013-1329-x>
- Uttayarat, P., Toworfe, G. K., Dietrich, F., Lelkes, P. I., & Composto, R. J. (2005). Topographic guidance of endothelial cells on silicone surfaces with micro- to nanogrooves: Orientation of actin filaments and focal adhesions. *Journal of Biomedical Materials Research Part A*, *75A*(3), 668–680.
<https://doi.org/10.1002/jbm.a.30478>
- van Delft, F., van den Heuvel, F. C., Loesberg, W. A., Riet, J. T., Schon, P., Figdor, C. G., ... Scho, P. (2008). Manufacturing substrate nano-grooves for studying cell alignment and adhesion (Vol. 85, pp. 1362–1366). Elsevier Science Bv.
<https://doi.org/10.1016/j.mee.2008.01.028>
- Vernerey, F. J., & Farsad, M. (2011). A constrained mixture approach to mechanosensing and force generation in contractile cells. *Journal of the Mechanical Behavior of Biomedical Materials*, *4*(8), 1683–1699.
<https://doi.org/10.1016/j.jmbbm.2011.05.022>
- Vincent, L. G., Choi, Y. S., Alonso-Latorre, B., del Alamo, J. C., & Engler, A. J. (2013). Mesenchymal stem cell durotaxis depends on substrate stiffness gradient strength. *Biotechnology Journal*, *8*(4), 472–484.

<https://doi.org/10.1002/biot.201200205>

- Vogel, V., & Sheetz, M. (2006). Local force and geometry sensing regulate cell functions. *Nat Rev Mol Cell Biol*, 7(4), 265–275.
- Walcott, S., & Sun, S. X. (2010). A mechanical model of actin stress fiber formation and substrate elasticity sensing in adherent cells. *Proceedings of the National Academy of Sciences of the United States of America*, 107(17), 7757–7762.
<https://doi.org/10.1073/pnas.0912739107>
- Wang, H. B., Dembo, M., Hanks, S. K., & Wang, Y. (2001). Focal adhesion kinase is involved in mechanosensing during fibroblast migration. *Proceedings of the National Academy of Sciences of the United States of America*, 98(20), 11295–11300. <https://doi.org/10.1073/pnas.201201198>
- Wedlich-Soldner, R., Altschuler, S., Wu, L., & Li, R. (2003). Spontaneous cell polarization through actomyosin-based delivery of the Cdc42 GTPase. *Science*, 299(5610), 1231–1235.
- Wong, S., Guo, W.-H., & Wang, Y.-L. (2014). Fibroblasts probe substrate rigidity with filopodia extensions before occupying an area. *Proceedings of the National Academy of Sciences*, 111(48), 17176–17181.
<https://doi.org/10.1073/pnas.1412285111>
- Wyczalkowski, M. A., Chen, Z., Filas, B. A., Varner, V. D., & Taber, L. A. (2012). Computational Models for Mechanics of Morphogenesis, 152(Part C), 132–152.
<https://doi.org/10.1002/bdrc.21013>
- Xiong, Y., Huang, C.-H., Iglesias, P. A., & Devreotes, P. N. (2010). Cells navigate with a local-excitation, global-inhibition-biased excitable network. *Proceedings*

- of the National Academy of Sciences*, 107(40), 17079–17086.
<https://doi.org/10.1073/pnas.1011271107>
- Yao, M., Qiu, W., Liu, R., Efremov, A. K., Cong, P., Seddiki, R., ... Yan, J. (2014). Force-dependent conformational switch of α -catenin controls vinculin binding. *Nature Communications*, 5. <https://doi.org/10.1038/ncomms5525>
- Yu, G., Feng, J., Man, H., & Levine, H. (2017). Phenomenological modeling of durotaxis. *Physical Review E*, 96(1), 1–6.
<https://doi.org/10.1103/PhysRevE.96.010402>
- Yuan, H., & Gao, H. (2012). On the mechanics of integrin clustering during cell-substrate adhesion. *Acta Mechanica Solida Sinica*, 25(5), 467–472.
[https://doi.org/10.1016/S0894-9166\(12\)60041-X](https://doi.org/10.1016/S0894-9166(12)60041-X)
- Yuan, H., Marzban, B., & Parker, K. K. (2017). Myofibrils in Cardiomyocytes Tend to Assemble Along the Maximal Principle Stress Directions. *Journal of Biomechanical Engineering*, 139(12). <https://doi.org/10.1115/1.4037795>
- Yuan, H., Marzban, B., & Parker, K. K. (2017a). Myofibrils in Cardiomyocytes Tend to Assemble Along the Maximal Principle Stress Directions. *Journal of Biomechanical Engineering*, 139(December 2017), 1–8.
<https://doi.org/10.1115/1.4037795>
- Yuan, H., Marzban, B., & Parker, K. K. (2017b). Myofibrils in Cardiomyocytes Tend to Assemble Along the Maximal Principle Stress Directions. *J Biomech Eng*, doi: 10.1115/1.4037795
- Zaman, M. H., Kamm, R. D., Matsudaira, P., & Lauffenburger, D. a. (2005). Computational model for cell migration in three-dimensional matrices. *Biophys J*,

89(2), 1389–1397. <https://doi.org/10.1529/biophysj.105.060723>

Zemel, A., Rehfeldt, F., Brown, A. E. X., Discher, D. E., & Safran, S. A. (2010a). Cell shape, spreading symmetry, and the polarization of stress-fibers in cells. *Journal of Physics: Condensed Matter*, 22(19), 194110. <https://doi.org/10.1088/0953-8984/22/19/194110>

Zemel, A., Rehfeldt, F., Brown, A. E. X., Discher, D. E., & Safran, S. A. (2010b). Optimal matrix rigidity for stress-fibre polarization in stem cells. *Nat Phys*, 6(6), 468–473. Journal Article. <https://doi.org/http://www.nature.com/nphys/journal/v6/n6/abs/nphys1613.html#supplementary-information>

Zeng, X., & Li, S. (2011). Multiscale modeling and simulation of soft adhesion and contact of stem cells. *Journal of the Mechanical Behavior of Biomedical Materials*, 4(2), 180–189. <https://doi.org/10.1016/j.jmbbm.2010.06.002>

Zienkiewicz, O. C., Taylor, R. L., & Zhu, J. Z. (2005). *The Finite Element Method: its Basis and Fundamentals. The Finite Element Method: its Basis and Fundamentals*. <https://doi.org/10.1016/B978-1-85617-633-0.00015-0>